

Marine Geophysical Research

March 2011, Volume 32 (1-2), Pages 225-243

<http://dx.doi.org/10.1007/s11001-011-9123-3>

© 2011, Springer Science+Business Media B.V.

Archimer
<http://archimer.ifremer.fr>

The original publication is available at <http://www.springerlink.com>

Morphology, distribution and origin of recent submarine landslides of the Ligurian Margin (North-western Mediterranean): some insights into geohazard assessment

Sébastien Migeon^{1,*}, Antonio Cattaneo², Virginie Hassoun¹, Christophe Larroque³, Nicola Corradi⁴,
Francesco Fanucci⁵, Alexandre Dano¹, Bernard Mercier de Lepinay³, Françoise Sage¹
and Christian Gorini⁶

¹ UMR GéoAzur, Université de Nice-Sophia Antipolis, CNRS, OCA, Port de la darse, 06235 Villefrance/Mer, France

² IFREMER, GM-LES, 29280 Plouzané, France

³ UMR GéoAzur, Université de Nice-Sophia Antipolis, CNRS, OCA, 250 Rue A. Einstein, 06560 Valbonne, France

⁴ University of Genova, Dip.Te.Ris, Corso Europa, 26 16100 Genova, Italy

⁵ University of Trieste, DiGe, Italy

⁶ UMR ISTeP, Université Pierre et Marie Curie, 4 Place Jussieu, 75252, Paris cedex05, France

*: Corresponding author : Sébastien Migeon, email address : migeon@geoazur.obs-vlfr.fr

Abstract :

Based on new multibeam bathymetric data, seismic-reflection profiles and side-scan sonar images, a great number of submarine failures of various types and sizes was identified along the northern margin of the Ligurian Basin and characterized with 3 distinct end-members concerning their location on the margin, sedimentary processes and possible triggering mechanisms. They include superficial landslides mainly located in the vicinity of the main mountain-supplied rivers and on the inner walls of canyons (typically smaller than 10^8 m³ in volume: Type 1), deep scars 100–500 m high along the base of the continental slope (Type 2), and large-scale scars and Mass Transport Deposits (MTDs) affecting the upper part of the slope (Type 3 failures). The MTDs are located in different environmental contexts of the margin, including the deep Var Sedimentary Ridge (VSR) and the upper part of the continental slope in the Gulf of Genova (Finale Slide and Portofino Slide), with volumes of missing sediment reaching up to 1.5×10^9 m³. High sedimentation rates related to hyperpycnal flows, faults and earthquake activity, together with sea-level fluctuations are the main factors invoked to explain the distribution and sizes of these different failure types.

Keywords : Ligurian Sea ; Submarine landslides ; Seafloor morphology ; Seismic-reflection profiles ; Side-scan sonar

33 **1. Introduction**

34 Submarine failures have been described with increasing details, especially during the last two
35 decades, in a wide range of climatic and tectonic settings, from glacial to subequatorial areas
36 [*Huhnerbach and Masson, 2004; Imbo et al., 2003; Laberg et al., 2000; McAdoo et al., 2000;*
37 *Piper et al., 1997*] and along both passive and active margins [*Collot et al., 2001; Goldfinger et*
38 *al., 2000; Moore et al., 1989; Urgeles et al., 1997*]. Triggering factors are, consequently, as
39 diverse as sea-level fluctuations, earthquakes, high-sediment supply leading to the overload of
40 under-consolidated deposits, fluid charging and more [*Sultan et al., 2004b*]. Depending on their
41 size and location on a margin, submarine failures could be responsible for various hazards
42 including tsunami and destruction of infrastructures such as submarine cables [*Fine et al., 2005;*
43 *Kvalstad, 2007; McAdoo and Watts, 2004; Piper et al., 1999*].

44 The interpretation of seafloor morphology in terms of mass wasting processes and the
45 identification of the potential factors controlling sediment failure are of major importance for the
46 geohazard assessment in a given area. The Mediterranean margins, which are tectonically active,
47 have a steep morphology and are fed by small mountain-supplied rivers, are highly affected by
48 severe landsliding processes. The Ligurian Basin experienced recently such phenomena: in 1979,
49 a submarine failure ($8 \times 10^6 \text{ m}^3$) occurred in shallow-water depth during infilling operations
50 seaward of the Nice airport [*Gennesseaux et al., 1980*] and generated three successive waves, 2-
51 3 m high, that broke along the coastline between the cities of Nice and Antibes. Three historical
52 tsunamis are also well-known in the area (1564, 1818, 1887 AD) and are closely related to
53 historical earthquake events. Earthquakes could have been responsible for tsunamogenic failures
54 in the Ligurian Sea, as previously described in other margin settings [*Fryer et al., 2004; Lòpez-*
55 *Venegas et al., 2008*].

56 The present study focuses on the northern margin of the Ligurian Sea where more than 500
57 submarine failures of various sizes have been identified on the continental slope between the
58 cities of Nice (France) and Genova (Italy). To analyse their morphologies and distribution on the
59 slope, and to identify their triggering mechanisms, a large dataset including Simrad EM300
60 multibeam bathymetry, seismic-reflection profiles, echo-sounder profiles and deep-tow side-scan
61 sonar was acquired in the frame of the MALISAR cruises (2006, 2007, 2008). Our goal is to
62 present the characters of the continental slope to outline the main features of the submarine
63 failures and factors controlling their distribution. These results will help improving our ability to

64 predict such geohazards along the Ligurian Margin and every margins with a similar
65 environmental context.

66

67 **2. Geological Setting**

68 2.1. Morphology of the margin and sediment supply

69 Along the northern margin of the Ligurian Sea, the continental-shelf width ranges from a
70 maximum of 2 km to less than 200 m at specific location like along the “Baie des Anges”, in
71 front of the city of Nice. The shelf break is thus located close to the coastline, at 50-100 m of
72 water depth as an average but could be much shallower, i.e. less than 20 m of water depth, like in
73 front of the Nice airport [Dan *et al.*, 2007]. The continental slope is steep and extends over 20 km
74 to a water depth of 2000 m with an average angle of 11° [Cochonat *et al.*, 1993]. The base of the
75 slope is characterised by a sharp decrease of the slope angle, to less than 3°. In the deep part of
76 the basin (2600 m of water depth), the slope angle decreases to 1° or less.

77 The main sedimentary accumulation of the Ligurian Margin is the Var turbidite system,
78 extending from the coastline offshore Nice to the Corsica island [Migeon *et al.*, 2006; Savoye *et*
79 *al.*, 1993]. Particles are delivered to the Var system through two canyons, the Var and Paillon
80 canyons, directly connected to rivers on land. Sediments are then distributed on the slope via
81 gravity-flow processes or via the decantation of surface plumes [Klaucke *et al.*, 2000]. The Var
82 and Paillon canyons coalesce at 1600 m of water depth and merge into a single submarine valley
83 about 170-km long [Migeon *et al.*, 2006]. In its middle part, the Var Valley exhibits an East-West
84 trend, and it is bordered to the south by a thick sediment accumulation, the Var Sedimentary
85 Ridge.

86 Although the present-day morphology of the margin mainly results from Plio-Quaternary
87 sedimentary processes, it has also been shaped by a sea-level lowering of about 1500 m during
88 the Messinian Salinity Crisis (~5.96-5.32 Ma). The Messinian deposits marks a relevant step in
89 the geological history of the Mediterranean. Their depocenter is partially controlled by inherited
90 morphology, as demonstrated in cases where the pre-Messinian deposits are imaged in seismic
91 profiles [Bertoni and Carthwright, 2006; Strzeczynski *et al.*, 2010]. On the Mediterranean
92 margins, the Messinian sea-level lowering was responsible for the incision of canyons on the
93 slope and the deposition of conglomerates at the base of the slope [Lofi *et al.*, 2005; Sage *et al.*,
94 2005]. In the deep basin, it resulted in the deposition of thick evaporite layers [Hsu *et al.*, 1973].

95 The northern Ligurian margin is fed by numerous small mountain-supplied rivers, like the Var,
96 Paillon, Roya, Taggia, Argentina, Arroscia, and Lavagna rivers. The largest one, the Var river,
97 forms in the southwestern Alps, at 2352 m of altitude and 120 km inland, and drains a 2822 km²
98 catchment basin [Mulder *et al.*, 1996]. These rivers experience abrupt flash floods during fall and
99 spring seasons. The average water discharge of the Var river, about 50 m³/s, can increase tenfold
100 during floods, and suspended sediment concentration can reach tens of kg/m³. From the rating
101 curve of the Var river, [Mulder *et al.*, 1998] estimated that hyperpycnal currents could be
102 generated during river floods, with a return period of about 2 to 5 years. Such turbulent flows are
103 generated at river mouth when the density of fresh water transporting suspended particles exceeds
104 the density of the ambient sea water. Thick fine-grained beds resulting from surface-plume
105 deposition [Klaucke *et al.*, 2000], and coarser but thinner inversely graded beds resulting from
106 hyperpycnal flows [Mulder *et al.*, 2001a] have been described on the slope offshore of Nice, as
107 well as at greater water depth in the basin [Migeon *et al.*, 2001]. Sedimentation rates related to
108 the activity of hyperpycnal flows can be as high as 1-2 m/100 years [Mulder *et al.*, 2001b]

109

110 2.2. Seismotectonic setting

111 The Ligurian basin is thought to originate from backarc extension related to the convergence
112 between the European and African plates [Jolivet and Faccenna, 2000]. The Oligo-Miocene
113 Ligurian rifting phase was followed by oceanic accretion between 20.5 and 18-15 Ma,
114 responsible for the 30° counterclockwise rotation of the Corsica-Sardinia block [Réhault *et al.*,
115 1984; Rollet *et al.*, 2002]. On land, some ancient and active faults exhibit a NW-SE trend
116 corresponding to the direction of transfer faults that guided the rifting [Larroque *et al.*, 2001]. At
117 sea, the continuity of the faults has not already been observed but the steep margin is incised by
118 numerous canyons that could follow their direction [Chaumillon *et al.*, 1994].

119 Historical and instrumental seismicity is mainly located in the western part of the Ligurian
120 margin (from the Cap Ferrat to Imperia), from the coastline to the base of the continental slope
121 [Courboulex *et al.*, 1998; Eva *et al.*, 2001; Larroque *et al.*, this issue]. Some earthquake
122 epicentres correlate with the location of faults and probably originated between 5 and 15 km
123 below the seafloor [Courboulex *et al.*, 1998]. The southwestern Alps and the continental margin
124 from Nice to Imperia experiences a recurrent seismic activity mainly characterised by several
125 moderate and some strong historical earthquake events (1564 AD, Intensity MKS I=IX-X; 1644

126 AD, I=VIII; 1818 AD, I=VIII; 1887 AD, I=X) and recent events (1963 AD, Magnitude M=6.0;
127 1981 AD, M=4.5; 1985 AD, M=4.1; 1989 AD, M=4.5; 1995 AD, M=4.7; 2001 AD, M=4.6;
128 [Bakun and Scotti, 2006; Chaumillon et al., 1994; Larroque et al., 2009]). For the 1887 Ligurian
129 earthquake, the macroseismic equivalent of magnitude has been estimated between 6.2 and 6.7
130 [Bakun and Scotti, 2006; Ferrari, 1991]. Among the most recent earthquakes, some of them like
131 the 1963, 1989, 1995 and 2001 events attest for reverse and strike-slip faulting [Courboulex et
132 al., 1998]. This suggests a tectonic inversion of the margin implying reactivation of inherited
133 transverse structures and development of new faults [Béthoux et al., 2008; Béthoux et al., 1992;
134 Larroque et al., 2009]. This tectonic reactivation is responsible for an uplift of the margin that is
135 mainly pronounced offshore the city of Imperia (Italy) [Bigot-Cormier et al., 2004].

136

137 **3. Methods and Data**

138 The dataset presented here was collected in the frame of the MALISAR Project. Three cruises
139 were conducted in 2006, 2007 and 2008 along the whole Ligurian margin, from the city of Nice
140 (France) to the Gulf of Genova (Italy) onboard R/V Le Suroît.

141 Multibeam bathymetry was collected using a Simrad EM300 and GPS-based navigation. Raw
142 bathymetric data were processed and merged using the Caraibes software (Ifremer, France) to
143 build a DTM with a spatial resolution of 25 m (Fig. 1). Bathymetric surveys covered the whole
144 margin between 100 and 2500 m water depth. The general bathymetric map allowed a detailed
145 study of seafloor morphology and the identification of mass-wasting related features. As
146 headwall scars of submarine landslides are well defined on bathymetric data, it was possible to
147 calculate the volume of sediment missing in some scars by reconstructing the pre-slide seafloor
148 topography and subtracting the pre- and post-slided surfaces with the Caraibes and GMT
149 software.

150 Side-scan sonar images and 3.5 kHz echo-sounder profiles were collected using the deep-towed
151 SAR (Système Acoustique Remorqué) system developed by Ifremer for very high-resolution
152 investigations of seafloor texture and micromorphology for water depths ranging from 200 to
153 6000 m. The SAR is a side-scan sonar towed about 80-100 m above the seafloor, at an average
154 speed of 1 ms⁻¹ (2 knots). The system provides a 1500-m wide swath of the seafloor with a
155 spatial resolution of 25 cm, and 3.5 kHz profiles with a vertical resolution of about 80 cm.

156 The internal architecture of slope deposits, failure scars and mass-transport deposits have

157 been studied using (1) Chirp profiles collected using a hull-mounted system (3 to 5 kHz) during
158 the bathymetric surveys, and (2) seismic-reflection profiles of various resolution collected
159 using a 300-m long 24-channels streamer and two mini-GI air gun (one 75/75 ci and one
160 40/40 ci), and a 450-m long 72-channels streamer and six mini-GI air gun (three 25/25 ci and
161 three 15/15 ci). Additional seismic-reflection profiles were collected during geophysical
162 training cruises conducted by the Villefranche-sur-Mer marine station. The data were recorded
163 using a 250 m-long 6-channel streamer and the seismic source was a mini-GI air-gun.

164

165 **4. Results**

166 4.1. General morphology of the Ligurian margin

167 Based on morphological characteristics, the Ligurian margin was divided in a western and an
168 eastern segment separated by a SW-NE trending ridge called the Imperia Promontory (Fig. 1;
169 Larroque et al., this issue). The study area comprises several morphologic domains that are
170 briefly described below:

171 - Seventeen canyons erode the continental slope from the city of Nice to the Gulf of Genova.
172 From west to east, they are the Var, Paillon, Roya, Nervia, Taggia, Verde, Mercula, Laigueglia,
173 Cuenta, Varatella, Pora, Finale, Noli, Vado, Polcevera, Bisagno and Levante Canyons.
174 Canyons initiate either at shallow water depth, directly at the mouth of some of the rivers
175 feeding the Ligurian continental slope and basin, or at greater depth, along the outer
176 continental shelf or on the upper continental slope. Along the western segment (Fig. 1),
177 canyons are mainly straight and perpendicular to the direction of the margin. Along the eastern
178 segment (Fig. 1), the Mercula and Laigueglia Canyons exhibit an unusual parallel direction to
179 the margin that is clearly constrained by the presence of the Imperia Promontory. All the
180 canyons identified along the eastern segment merge at about 2000 m water depth into a larger
181 submarine valley called the Genova Submarine Valley.

182 - The Var Sedimentary Ridge (VSR) is a thick W-E elongate sediment accumulation
183 corresponding to the right-hand levee of the Var Valley (Figs 1 and 2) [Migeon et al., 2006]. It
184 lies at the base of the continental slope between 2100 and 2500 m water depth. The slope angle
185 varies from 10° on the inner flank (facing the Var Valley) to 2-3° on the outer flank. On seismic-
186 reflection profiles, the internal architecture of the Ridge show well-layered, low to moderate-
187 amplitude reflections corresponding to the rhythmic alternation of turbidites and hemipelagites

188 [Migeon *et al.*, 2006; Savoye *et al.*, 1993]. Several lenticular bodies, with high-amplitude
189 discontinuous to chaotic reflections and interpreted as paleochannels, are interbedded within the
190 well-layered seismic facies at several depths below the seafloor [Migeon *et al.*, 2006; Savoye *et*
191 *al.*, 1993]. The VSR built on top of the thick evaporite layer deposited during the Messinian
192 Salinity Crisis [Savoye *et al.*, 1993].

193 - Numerous remarkable large-scale failure scars affect the base of the continental slope along the
194 western segment (Fig. 1). Similar scars are absent from the eastern segment. The different types
195 of slope instabilities, their distribution and potential triggering factors are described and
196 discussed below.

197 - Several fault scarps tens of meters high, with a SW-NE trend, are located at the base of the
198 continental slope or at greater depth in the basin, south of the Imperia Promontory (Fig. 1). The
199 relationship between these faults and the deformation and seismicity of the Ligurian margin is
200 discussed by Larroque *et al.* (this issue).

201 The main geohazards identified by means of multibeam bathymetry and geophysical data are
202 failure scars and faults. The integration of observations coming from bathymetric data side-
203 scan sonar images and seismic-reflection profiles allows us to distinguish three main Types of
204 slope failures along the northern Ligurian margin, based on the morphology, size and specific
205 location of scars on the continental slope.

206

207 4.2. Type 1 failure scars

208 Type-1 failure scars are mainly superficial and affect the uppermost 30 to 90 m of deposits
209 below the seafloor, representing volumes less than 10^8 m^3 on average (Table 1). The largest
210 number of Type-1 scars (about 200) was found on the upper slope in the vicinity of the main
211 feeding rivers, i.e. the Var and Paillon rivers (Fig. 2). This is the case of the so-called “Nice
212 1979” submarine landslide that was triggered at the transition between the outer continental shelf
213 and the upper continental slope (Fig. 3A) [Dan *et al.*, 2007]. There, the continental slope exhibits
214 a concave-up topographic profile (Fig. 1) and slope angle is 10 to 15°. Some Type-1 failure scars
215 are also located: (1) on the inner walls of most of the canyons eroding the continental slope,
216 where the slope angle exceeds 20°, and (2) on open slope environments, far from direct sediment
217 supply and canyons but close to earthquake-epicentral areas like the one of the 1887 earthquake,
218 where the slope angle is about 5°.

219 Whatever their location on the continental slope, Type-1 scars mainly exhibit an ellipsoidal or
220 amphitheatre-like morphology (Fig. 3). In some cases, scars are more complex, and consist of
221 several nested amphitheatre-like morphologies (Fig. 3B). Each scar is continuing on the slope by
222 a chute that evidences the erosive power of the failed mass remobilized in the scar (Fig. 3). The
223 chutes are essentially straight in the direction of the main slope angle in their downslope part,
224 whereas they exhibit a low-sinuosity pattern in their upstream part (Fig. 3A). They are few
225 hundred meters to 5-km long. The chutes show a width comparable with that of the scars in the
226 upper reach, then enlarge and deepen downslope. In most cases, on both bathymetric data and
227 Chirp profiles, Mass-Transport Deposits (MTD) are not found downstream from the scars, in the
228 chutes. A similar observation was made by [Klaucke and Cochonat, 1999] from the detailed
229 study of the Nice slope using SAR data. This suggests that the remobilized deposits are
230 completely evacuated to the base of the slope, in a manner similar to „disintegrative“ mass
231 failures [McAdoo et al., 2000]. Rare small-scale MTD were identified from the presence of
232 compressive ridges (Fig. 3B) and transparent echofacies. They are mainly located at the
233 transition between the canyon walls and the canyon floors where the slope angle decreases
234 rapidly.

235

236 4.3. Type 2 failure scars

237 Type 2 failure scars are large scars affecting the base of the continental slope, between 1700
238 and 2200 m of water depth (Fig. 2; Table 1). The best known example of such type of failure is
239 the so-called “Cirque Marcel” [Savoie and Piper, 1991]. Fourteen failures of Type 2 have
240 been identified along the 50-km long segment of the slope comprised between the cities of
241 Nice (France) and Imperia (Italy). Here, the continental slope exhibits a convex-up
242 topographic profile (Fig. 1). The location of scars correlates with the steepest part of the
243 continental slope, where the slope angle is of about 6°.

244 Type-2 scars are 2 to 4-km wide, 4 to 6-km long as an average. Volumes of remobilized deposits
245 decrease gradually eastward from $2\text{-}2.6 \times 10^9 \text{ m}^3$ to less than $25 \times 10^6 \text{ m}^3$. In plan view, they
246 exhibit a complex amphitheatre-like morphology resulting from several semi-circular nested
247 scars (Fig. 4). In the Cirque Marcel, from the top to the base, four scars are present with heights
248 ranging from 100 to 300 m. They are separated by flat areas 1 to 2-km wide. These areas exhibit
249 evidences of erosional processes, revealed by the presence of smaller-scale scars and scours

250 (Figs 4 and 5). The scars also exhibit semi-circular geometry on both bathymetric profiles (Fig.
251 4) and Chirp and 3.5 kHz (SAR) profiles (Fig. 5). Draping hemipelagic-like deposits are not
252 observed on 3.5 kHz (SAR) profiles (Fig. 5), suggesting recent phase of triggering or superficial
253 sediment removal by low-density gravity flows and bottom currents. Accumulations of
254 destabilized deposits are located at the foot of these structures, at the base of the continental
255 slope (Figs 4 and 5). They are 20 to up to 80 m in thickness and extend laterally over maximum
256 distances of 5 km. Rocky blocks, tens of meters in diameter, are scattered on top of these
257 accumulations (Fig. 5 and 6). For the Cirque Marcel, the volume of the accumulation is about
258 $1.3 \times 10^8 \text{ m}^3$, i.e. 20 times lower than the total volume of the missing sediment in the scar.
259 Seismic-reflection profiles suggest these large failure-related scars affected in most cases the
260 whole Plio-Quaternary section, 300 to 500-m thick, and the slip plans correlate with the top of
261 the Messinian conglomerates (Fig. 7). In the “Cirque Marcel”, this interpretation is supported by
262 direct observation reporting the presence of messinian-conglomerates and pliocene-marl
263 outcrops within the main scars [Savoye and Piper, 1991].

264 In the area offshore Nice to Imperia, the base of the continental slope is also strongly affected by
265 faults (Figs 2 and 7). The deepest ones broke and shifted vertically the Messinian conglomerates,
266 but the penetration of the seismic-reflection profiles did not allow the observation of these faults
267 at greater depth (Fig. 7). Vertical displacements could be in the order of 300-400 ms (about 200-
268 300 m). The shallowest faults affect the Plio-Quaternary deposits: some of them are visible on
269 side-scan sonar images of the seafloor (Fig. 6), suggesting a recent activity. Vertical
270 displacements along these faults are less than 50 ms (about 40 m).

271
272 4.4. Type 3 Failure scars
273 Type-3 failures are more superficial than failures of Type 2 but affect wider areas and rework
274 larger volumes of pre-existing deposits (Table 1). They are located in different environmental
275 contexts of the margin, including the deep Var Sedimentary Ridge (VSR) and the upper part of
276 the continental slope in the Gulf of Genova. In contrast with Type-1 and -2 failures previously
277 described, Type-3 scars are also associated with the presence of mass-transport deposits.

278
279 *The VSR Slide* – The VSR slide is located in the western part of the outer flank of the VSR (Fig.
280 8). It consists of a main scar 6-km wide and 100-m high that gradually smooths to the west. It

281 was generated along the crest of the Ridge, at about 1800 m of water depth, and it extends
282 downslope to 2100 m of water depth. The inner wall of the main scar is affected by smaller-scale
283 failures, 0.5- to 1-km wide, separated by elongated ridges (Fig. 8). The ridges probably consist of
284 poorly disturbed material as coherent and continuous reflections are still observed (Figs 9 and
285 10). The volume of missing sediment in the whole failure-related area is of $1.5 \times 10^9 \text{ m}^3$.

286 A lenticular-shaped chaotic to transparent unit deposited at least 12 km downstream from the scar
287 (Fig. 11): it is interpreted as a mass-transport deposit (MTD). The MTD is up to 20 m in
288 thickness and 2-3 km wide. Its basal contact is erosive, as evidenced by the truncation of
289 reflectors of the well-layered echofacies corresponding to the VSR deposits (Fig. 11). Erosion
290 affected locally up to 5-10 m of VSR deposits. The MTD is draped by hemipelagic-like deposits
291 5-m thick (Fig. 11). By assuming a sedimentation rate of 17 cm/1000 yrs in that part of the VSR
292 [Piper and Savoye, 1993], the age of the MTD could be about 29-30 ka BP.

293 The VSR Slide is located above a network of syn-sedimentary faults exhibiting a flower-like
294 pattern and affecting the upper 400 ms of sediment below the seafloor (Fig. 9). The lateral limits
295 of the scar correlate with faults reaching the seafloor (Figs 9 and 10). The apparent vertical
296 displacement along these faults suggests that the whole failure area subsided within the
297 surrounding deposits of the VSR. The superficial faults gradually converge at depth and are
298 located above some larger-scale faults that affect the paleo-channels and are rooted on top of the
299 Messinian evaporites (Figs 9 and 10). Vertical displacements along these deep faults are about
300 50 to 200 ms (about 55 to 220 m).

301
302 *The Finale Slide* – The Finale Slide was identified in the northwestern part of the Gulf of
303 Genova during the MALISAR1 cruise (Fig. 12). It is located on an interfluvial area where the
304 Pora and Noli Canyons coalesce (Fig. 13). Here, the slope angle is about 4° . The scar lies at 700
305 m water depth. It is 10-km wide, 3-km long and 50-m high as an average. The volume of
306 missing sediment in the scar is of $1.5 \times 10^9 \text{ m}^3$. Two superficial semi-circular failures with
307 volume lower than 10^5 m^3 affected the scar in its eastern part (Fig. 13). A chaotic to transparent
308 body deposited in the continuity of the scar and reached the Noli Canyon (Fig. 14). It is
309 interpreted as a MTD resulting from the transformation of the destabilized deposits. The MTD is
310 about 20-30 m thick near the base of the scar and it thins to 10-15 m in the Noli Canyon (Fig.
311 14). Draping hemipelagic-like deposits are not observed on top of the MTD on Chirp profiles,

312 suggesting a recent emplacement.

313
314 *The Portofino Slide* – The Portofino slide was first identified on Sparker profiles by [Corradi et
315 al., 2001] and its western part was mapped during the MALISAR2 cruise. It is located in the
316 northeastern part of the Gulf of Genova (Fig. 12), on the upper continental slope where the mean
317 slope angle is about 3°. The scar lies at about 250 m water depth. It consists of a sharp
318 escarpment (slope angle of about 7°) 300-m high followed at its base by a MTD about 200-m
319 thick. The volume of missing sediment was not evaluated in that case as the scar was
320 incompletely mapped. The MTD extend about 10 km downstream from the scar (Fig. 12). Its
321 internal architecture partly exhibits the original organisation of deposits evidenced by the
322 presence of well-layered moderate-amplitude reflections [Corradi et al., 2001]. The change of
323 reflection dip along the whole MTD was interpreted by [Corradi et al., 2001] as a slight
324 rotational movement of the destabilized deposits. The distal part of the MTD is now eroded by
325 the Levante Canyon (Fig. 12). A field of pockmarks is located west of the Portofino Slide and
326 lies at a water depth ranging from 300 to 500 m (Fig. 12).

327

328 **5. Discussion**

329 The specific location of each Type of failure scars along the Ligurian Margin could give hints
330 on the controlling factors influencing their triggering, including the structure of the margin, the
331 presence of large faults, the areas of highest earthquake activity and of highest sedimentation
332 rate.

333

334 5.1. Single vs multiple-failure events

335 In terms of geohazard assessment, it is important to understand the processes leading to the
336 formation of the scar morphologies identified on the present-day seafloor. Depending on these
337 processes, estimation of volumes of deposits reworked on the continental slope or intensity of
338 slope-deposits erosion during a single event could differ totally and change our ability to estimate
339 the tsunamigenic potential of submarine failures.

340 Looking at the morphology of Type-1 failures, each erosional chute seems to have originated
341 from a single scar, suggesting that a single failure event triggered on the upper slope and evolved
342 downslope to an erosive cohesive mass-flow (Fig. 3). Within the chutes, the lack of mass-

343 transport deposits (MTD) suggests that when a failure is triggered, the remobilized deposits are
344 completely evacuated to the base of the slope. On the Nice slope, this interpretation is supported
345 by the fact that debris-flow deposits were only identified at the base of the slope, in two areas
346 close to the Var and Paillon Canyons [*Klaucke and Cochonat, 1999*].

347 For Type-3 failures, the presence of a single thick MTD downslope from the scar also suggests a
348 single failure event, although it is possible that the MTD characterises only one of the recorded
349 phases of failure. However, phases of seafloor erosion older than the one identified at the base of
350 the MTDs were not observed, suggesting that the MTDs are, at least, associated to the main
351 failure event. In the example of the VSR Slide (Fig. 8) and the Finale Slide (Fig. 13), secondary
352 small-scale failures are present within the main scar, but their volumes are too small to be
353 responsible for the emplacement of the large MTD identified downstream of the scars. These
354 secondary events are post-failure processes probably related to the local oversteepening created
355 along the scar together with the sediment decompression affecting the surrounding deposits. We
356 therefore infer that they generated directly on the main scar as it adjusted to a critical inclination
357 with a mechanism of retrogressive failure.

358 Along the western Ligurian margin, at the base of the continental slope, large-scale imbricated
359 scars of Type 2 are an evidence of multiple failure events. The presence of several scars showing
360 a step-like morphology results from several décollements that followed distinct stratigraphical
361 surfaces likely acting as mechanical discontinuities, like the surface between the consolidated
362 Pliocene marls and the Messinian conglomerates, and in few cases, the surface between the soft
363 Quaternary deposits and the Pliocene marls. The differences in physical properties of the
364 sedimentary units could have controlled the location and action of the shear stress within the
365 sedimentary column. It is still unclear whether several failure events were triggered in a very
366 short period of time or if distinct failure events affected successively the Messinian
367 conglomerates, then the Pliocene marls and the Quaternary deposits. The outstanding difference
368 between the volume of reworked deposits accumulated at the base of the scars and the volume of
369 missing deposits within the scars should favour the second hypothesis: large volumes of the
370 reworked-deposit accumulation could have been evacuated between two successive failure events
371 by thick and energetic gravity flows flowing into the Var Valley.

372

373 5.2. Factors promoting submarine failures along the Ligurian margin

374 Several factors may promote the distribution and triggering of submarine failures along the
375 Ligurian margin. Each factor may act differently in time and space but it is the conjunction of
376 all these parameters that controlled the failure emplacement. Undoubtedly, some factors
377 interact or are closely connected but, for clarity, we discuss their effect separately.

378
379 *Effect of slope angle.* The slope angle is known as an important factor controlling the location
380 and volume of submarine failures [Canals et al., 2004; McAdoo et al., 2000]. However, as
381 submarine landslides are found associated with a large spectrum of slope angles, the slope
382 angle is not always considered as a good indicator of susceptibility to landsliding [Huhnerbach
383 and Masson, 2004]. Along the Ligurian margin, areas with smallest-scale but more abundant
384 failures (Type-1 failures) correlate with areas of highest slope angle (10-20°) like the upper
385 continental slope offshore the Var-river mouth and the inner canyon walls (Fig. 2). Areas with
386 large-scale but rarer failures are located on lower slope angle, of about 5-6° (Type-2 failure
387 scars) and 2-4° (Type-3 failure scars). Similar inverse correlation between the slope angle and
388 the size of failures was made along the US continental margins [McAdoo et al., 2000] and the
389 North Atlantic margins [Huhnerbach and Masson, 2004]. Because high slope angle will
390 promote regular failure events, it will also prevent thick unstable sediment accumulation to
391 build through time. In that case, only small volume of continental-slope deposits will be
392 remobilized during each failure event, as it is observed along similar steep margins of the
393 Mediterranean, like the Algerian margin [Cattaneo et al., 2010].

394 Slope angle might also play an important role on the post-failure processes and the
395 transformation of a failed mass into a gravity flow. Mass-transport deposits are never found
396 immediately downslope of Type-1 and Type-2 scars, or they are found far from these scars
397 where the slope angle decreases drastically (Fig. 5), while MTDs are always found
398 downstream of Type-3 scars. This suggests that slope angles greater than 5-6° should promote
399 a complete disintegration and evacuation of the failed mass while slope angles lower than 4°
400 should conserve the cohesion of the failed mass. One possible interpretation could come from
401 a difference in the rheology of the material that could be stiffer and more consolidated on
402 gentler slopes and softer and less consolidated on steeper slopes, also as a consequence of the
403 shorter time of residence/accumulation of sediment in very steep settings. High slope angles
404 could also promote a rapid acceleration of the failed mass just after the failure occurred, what

405 should increase the process of disintegration.

406

407 *Effect of sedimentation rates and hyperpycnal currents.* Sedimentation rates are high in the
408 surrounding areas of the mouths of the main feeding rivers like the Var, the Paillon, the Roya,
409 the Taggia. There, sediment deposition mainly results from both direct and rapid supply by
410 hyperpycnal flows, inducing sedimentation rates as high as 1-2 m/100 yrs [Mulder *et al.*,
411 2001b], then by slower decantation of surface plumes [Klaucke *et al.*, 2000]. Geotechnical
412 analyses described these deposits as underconsolidated [Cochonat *et al.*, 1993]. Due to angles of
413 10-15°, failures of Type 1 are thought to occur regularly, but small volumes of deposits are
414 involved for each episodes of failure. Hyperpycnal flows could have a direct impact on the
415 seafloor and the triggering of small-scale failures through mechanisms of friction at the seabed
416 creating a temporary additional loading. They are also involved in the gradual erosion of the
417 base of the canyon walls, leading to local oversteepening responsible for the triggering of
418 failures of Type 1 (e.g. [Baztan *et al.*, 2005]).

419

420 *Effect of uplift, inherited structural features and earthquakes.* The triggering of landslides is
421 commonly associated to earthquakes on the North Atlantic margin [Piper *et al.*, 1999; St-Onge
422 *et al.*, 2004; ten Brink *et al.*, 2009], in the Mediterranean [Cattaneo *et al.*, 2010; Hassoun *et al.*,
423 2009; Lastras *et al.*, 2004] and in the Pacific [Lamarche *et al.*, 2008]. On the eastern Canadian
424 margin, [Piper *et al.*, 2003] interpret large buried landslides to largely result from earthquakes.
425 In the western Ligurian margin (Fig. 2), the location of Type-2 failures at the base of the
426 continental slope is uncommon: on passive margins, large-scale failures are usually triggered on
427 the upper continental slope where the slope angle and the thickness of deposits are the highest
428 [Garziglia *et al.*, 2008; Haflidason *et al.*, 2004; McAdoo *et al.*, 2000]. In the western Ligurian
429 margin, the specific location of failure morphologies correlates with the presence of numerous
430 faults affecting the base of the slope (Figs 2, 6 and 7). The origin of these faults is still discussed
431 [Larroque *et al.*, this issue], but they induced through time a total vertical displacement of at least
432 300 m (Fig. 7). At sea, most of the earthquake epicentres are located on these structures
433 [Courboulex *et al.*, 1998; Larroque *et al.*, this issue]. As strong vertical displacement along faults
434 usually correlates with earthquakes, the triggering of large collapses of Type 2 could result from
435 earthquakes and the combined effect of ground rupture along faults and cyclic loading affecting

436 the sediment cover. In addition, that part of the margin also experience a present-day
437 deformation/uplifting stage starting during the Pliocene [*Bigot-Cormier et al.*, 2004]. The uplift is
438 responsible for the gradual oversteepening of the margin, resulting in a progressively more
439 marked convex-up morphologic profile (Fig. 1). As the margin exhibits seaward dipping strata
440 (Fig. 7), it may require less energy under these conditions to generate a failure during
441 earthquakes.

442 The strongest earthquake events are also probably responsible for the direct and rapid
443 triggering of landslides through processes of shacking and loading, as for failures of Type 1
444 identified in the open-continental-slope epicentral area of the 1887 event [*Hassoun et al.*,
445 2009], or for the large Finale Slide that triggered on low slope angle. It is possible that the
446 presence of layers or surfaces of contrasting lithology, like the coarser layers that are prone to
447 liquefaction during earthquakes, provide preferential weak planes where failure may originate.

448
449 *Effect of the presence of a mobile evaporite layer.* The large failure event identified in the
450 western part of the VSR locates in an area where the low slope angle and the low sedimentation
451 rates should not have favoured its development. It is also located above a fault network that roots
452 into the Messinian evaporites (Figs 9 and 10). All over the Mediterranean Sea, the Messinian
453 evaporites are considered as a mobile layer that affect the overlying Plio-Quaternary succession
454 in numerous ways [*Masclé et al.*, 2006]. The main processes evoked include the thin-skinned
455 gravitational tectonics linked to salt withdrawal (downdip migration or dissolution) of the
456 evaporites as evidenced on recent high-resolution 2D data offshore Algeria [*Strzeczynski et al.*,
457 2010] and 3D data offshore Israel (e.g., [*Bertoni and Cartwright*, 2006]). As a thick sediment
458 accumulation, the VSR exerted a strong lithostatic pressure on the evaporites that gradually
459 glided to the south following the regional slope gradient. This is evidenced by the thickening of
460 the salt layer and the presence of salt diapirs along the southern border of the VSR, where the
461 sediment accumulation thins out [*Savoie et al.*, 1993]. The slow downslope movement of the
462 evaporite layer resulted in a decompression at depth and the formation of normal syn-sedimentary
463 faults that gradually propagated upward (Figs 9 and 10). Both decompression and faults affected
464 the Plio-Quaternary deposits that subsided rapidly, triggering the destabilisation of the seafloor.

465
466 *Effect of sea-level fluctuation.* On passive margins, the triggering of large-scale failures is

467 quite often closely connected to phases of sea-level rising or lowering [*Garziglia et al.*, 2008;
468 *Maslin et al.*, 2005]. Sea-level changes can act on slope instability through several processes
469 like seaward migration of the main sediment depocenters leading to an increasing
470 sedimentation rate on the continental slope together with a rapid sediment loading, change of
471 the physical properties of deposits experiencing an increase or decrease of their excess pore
472 pressure, and dissociation of gas hydrates. In the absence of direct dating, it can be only
473 speculated that large failures triggered at shallow water depth, like the Portofino Slide
474 affecting segment about 5-km long of the upper slope, could have been triggered by the latest
475 phases of sea-level lowering or rising of about 110 m, during the Last Glacial Maximum or the
476 early Holocene respectively [*Lambeck and Purcell*, 2005]. The Portofino Slide being located
477 far from direct sources of sediment supply, seaward migration of depocenters and sediment
478 overloading on the upper continental slope during the latest phase of lowered sea level should
479 not be responsible for the triggering of that large failure. Decomposition of gas hydrates is
480 known to trigger large-scale landslides during phases of sea-level lowering, mainly if they
481 occur on the upper continental slope [*Maslin et al.*, 2004; *Sultan et al.*, 2004a]. In the present
482 case, evidence of bottom simulating reflector (BSR) as an indicator of gas hydrates in the
483 deposits was not yet observed on seismic-reflection profiles from the Ligurian margin but the
484 field of pockmarks located at a similar water depth than the Portofino Slide (Fig. 12) could be
485 an evidence of the potential dissociation of gas hydrates.

486

487 5.3. Impact on geohazard assessment

488 Along the Ligurian margin, factors promoting submarine landslides act at specific locations.
489 Correlation between the types of factors and the types of submarine failures could help to
490 discriminate between areas that are prone to low-to-high geohazards.

491 Type-1 failure scars correlate with areas of both high slope angle and direct high particle-
492 supply by hyperpycnal flows. These two factors promote high-frequency failures, with
493 volumes classically lower than 10^8 m^3 . As these two factors are closely connected with river
494 discharges and seafloor erosion, these failures are restricted in small areas localized in the
495 vicinity of river mouths and on the inner flanks of canyons. As a consequence, they do not
496 strongly impact the morphology and the erosion of the whole margin. However, from the
497 example of the 1979 Nice-airport landslide, such failures are able to generate tsunami despite

498 their small volume because they occur at shallow water depth [Ioualalen *et al.*, 2010]. In the
499 case of the 1979 event, three waves less than 3-m high broke along the coastline between the
500 cities of Antibes and Nice less than 8 minutes after the failure occurred. Similar Type-1
501 failures triggering at shallow water depth are thus thought to generate low-elevation tsunami
502 affecting the coastline within a radius of 5-10 km around the point of sediment rupture and
503 within a very short-time period. Such failures are also able to rapidly transform into gravity
504 flows that can expand drastically through processes of seafloor erosion [Mulder *et al.*, 1997;
505 Piper and Savoye, 1993]. Their increasing volume and density allow these flows to transport
506 large volume of particles to the deep part of the margin and to break submarine cables more
507 than 100 km away from their source as it happened for the 1979 flow. Type-1 failures could
508 thus have a low-to-high hazard potential, not necessarily linked to regional seismicity as in the
509 case of the 1979 Nice event [Dan *et al.*, 2007].

510 Type-2 failure scars correlate with the uplifting area of the margin and with the presence of
511 main fault planes where earthquakes are also mainly concentrated. We infer that these three
512 factors are responsible for the triggering of low-to-mid frequency failures with large volumes,
513 ranging from 1 to 3 km³. These failures affect the base of the continental slope along the whole
514 western Ligurian margin (between E7°20'' and E8°10'' in longitude) and thus have a strong
515 impact on its evolution in time and space. Despite their location at water depth ranging from
516 1700 to 2000 m, such failures could potentially generate tsunami several metres high when
517 assuming the worst possible conditions in the tsunami-simulation scenario, i.e. remobilisation
518 of large volume ($> 10^9$ m³) during a single failure event [Ioualalen *et al.*, 2010]. As these
519 failures occurred about 20 km offshore from the coastline, the tsunami would be able to
520 propagate within the whole western Ligurian basin and to affect the coastline in an area 20-50
521 km long around the location of the failure [Ioualalen *et al.*, 2010]. Type-2 failures could thus
522 have a high hazard potential, especially in the scenario of single event, which is still difficult
523 to prove in the absence, in most cases, of clearly identifiable proximal MTDs or distal turbidite
524 deposits associated to the failure scars.

525 Type-3 failure scars are always associated to the presence of clearly identified MTDs and seem
526 to represent single main failure-events in which large volumes ($> 10^9$ m³) of deposits could
527 have been remobilized. The VSR slide is very deep (> 2000 m water depth), possibly
528 associated with the presence of deep faults, and, owing to its depth, unlikely to have generated

529 significant tsunami waves. The two large submarine landslides identified in the eastern
530 Ligurian margin (Finale and Portofino Slides) represent probably large events. Because they
531 triggered at 250-700 m water depth, these failures could have been responsible for significant
532 tsunami waves but more detailed investigations are still needed to assess their potential
533 geohazard.

534

535 **Conclusions**

536 Recent cruises conducted in the frame of the MALISAR project provided a huge dataset
537 including multibeam bathymetry, Chirp echo-sounder profiles, 24- and 72-channels seismic-
538 reflection profiles, and deep-tow side-scan sonar along the whole northern margin of the
539 Ligurian Basin, from the cities of Nice (France) to Genova (Italy). The dataset revealed that the
540 margin is affected by a remarkable number of slope instabilities of different morphologies and
541 sizes and allowed us to obtain a first order screening of the potential geohazards present in the
542 area.

543 The superficial failures of Type 1 are mainly located in the areas surrounding the mouth of the
544 mountain-supplied rivers like the Var and the Paillon rivers, and along the walls of canyons
545 eroding the continental slope. High sedimentation rates related to hyperpycnal flows and
546 gradual basal erosion of canyon walls are thought to be the main trigger mechanism of such
547 failures. By comparison with the effects of the 1979 Nice-airport landslides, Type-1 failures
548 with volume lower than 10^8 m^3 and occurring at shallow water depth could have a low-to-high
549 hazard potential.

550 Large scars corresponding to failures of Type 2 are located at the base of the continental slope,
551 between 1700 and 2200 m of water depth. Their location correlates with the presence of faults
552 that are also the areas of highest earthquake activity. They could result from multi-phase mass-
553 wasting events; however, the reconstruction of the timing of such events is still matter of an
554 open debate. Because large volumes (greater than 10^9 m^3) are potentially remobilized during
555 single failure events, Type-2 failures could have a high hazard potential.

556 Large-scale scars, affecting segment of the margins several kilometres long, and MTDs from
557 failures of Type 3 are located at different places along the Ligurian margin: on the upper part of
558 the continental slope or on the Var Ridge in the deep part of the Ligurian basin. Depending on
559 their locations, triggering factors for such landslides could be strong earthquakes, sea-level

560 fluctuations, and slow downslope movement of the mobile evaporite layer deposited in the deep
561 basin during the Messinian Salinity Crisis: a case-by-case approach with additional data is
562 probably necessary to assess the related geohazards for this last type of failures.

563

564 **Acknowledgement**

565 The authors would like to thank the captains and crew of the RV Le Suroît (Ifremer-Genavir)
566 and the RV Téthys II (INSU-CNRS). This work was funded by the French research programs
567 “GDR Marges”, “Reliefs de la Terre” and “Action Marges”. The final version of the manuscript
568 benefited from constructive suggestions and comments by Sam Johnson and an anonymous
569 reviewer.

570

571 **References**

- 572 Bakun, W. H., and O. Scotti (2006), Regional intensity attenuation models for France and the
573 estimation of magnitude and location of historical earthquakes, *Geophysical Journal*
574 *International*, 164, 596-610.
- 575 Baztan, J., S. Berné, J.-L. Olivet, M. Rabineau, D. Aslanian, M. Gaudin, J.-P. Réhault, and M.
576 Canals (2005), Axial incision: The key to understand submarine canyon evolution (in the
577 western Gulf of Lion), *Marine and Petroleum Geology*, 22, 805-826.
- 578 Bertoni, C., and J.A. Cartwright (2006), Controls on the basinwide architecture of late Miocene
579 (Messinian) evaporites on the Levant margin (Eastern Mediterranean), *Sedimentary*
580 *Geology*, 188/189, 93-114.
- 581 Béthoux, N., E. Tric, J. Chery, and M.-O. Beslier (2008), Why is the Ligurian basin
582 (Mediterranean sea) seismogenic? Thermomechanical modeling of a reactivated passive
583 margin, *Tectonics*, 27. TC5011, doi:10.1029/2007TC002232
- 584 Béthoux, N., J. Fréchet, F. Guyoton, F. Thouvenot, M. Cattaneo, E. Eva, B. Feignier, M.
585 Nicolas, and M. Granet (1992), A closing Ligurian Sea?, *Pure and Applied Geophysics*,
586 139(2), 179-194.
- 587 Bigot-Cormier, F., F. Sage, M. Sosson, J. Déverchère, M. Ferrandini, P. Guennoc, M. Popoff,
588 and J.-F. Stéphan (2004), Déformations pliocènes de la marge nord-Ligure (France) : les
589 conséquences d'un chevauchement crustal sud-alpin, *Bulletin de la Société Géologique de*
590 *France*, 175(2), 197-211.
- 591 Canals, M., et al. (2004), Slope failure dynamics and impacts from seafloor and shallow sub-
592 seafloor geophysical data: case studies from the COSTA project, *Marine Geology*, 213, 9-
593 72.
- 594 Cattaneo, A., et al. (2010), Submarine landslides along the Algerian margin: a review of their
595 occurrence and potential link with tectonic structures, in *Submarine Mass Movements and*
596 *Their Consequences - Advances in natural and Technological Hazards Research*, edited
597 by D. C. Mosher et al., Springer, 28, 541-552.
- 598 Chaumillon, E., J. Deverchère, J.-P. Réhault, and E. Gueguen (1994), Réactivation tectonique et
599 flexure de la marge continentale Ligure (Méditerranée Occidentale), *Comptes Rendus de*
600 *l'Académie des Sciences Paris*, 319, 675-682.

601 Cochonat, P., L. Dodd, J.-F. Bourillet, and B. Savoye (1993), Geotechnical characteristics and
602 instability of submarine slope sediments, the Nice slope (N-W Mediterranean Sea),
603 *Marine Georesources and Geotechnology*, *11*, 131-151.

604 Collot, J.-Y., K. Lewis, G. Lamarche, and S. Lallemand (2001), The giant Ruatoria debris
605 avalanche on the northern Hikurangi margin, New Zealand: result of oblique seamount
606 subduction, *Journal of Geophysical Research*, *106*(B9), 19271-19297.

607 Corradi, N., A. Cuppari, F. Fanucci, and D. Morelli (2001), Gravitative instability of
608 sedimentary masses on the Ligurian Sea margins, *GeoActa*, *1*, 37-44.

609 Courboux, F., A. Deschamps, M. Cattaneo, F. Costi, J. Déverchère, J. Virieux, P. Augliera, V.
610 Lanza, and D. Spallarossa (1998), Source study and tectonic implications of the 1995
611 Ventimiglia (border of Italy and France) earthquake (M = 4.7), *Tectonophysics*, *290*, 245-
612 257.

613 Dan, G., N. Sultan, and B. Savoye (2007), The 1979 Nice harbour catastrophe revisited: Trigger
614 mechanism inferred from geotechnical measurements and numerical modelling, *Marine*
615 *Geology*, *245*, 40-64.

616 Eva, E., S. Solarino, and D. Spallarossa (2001), Seismicity and crustal structure beneath the
617 western Ligurian Sea derived from local earthquake tomography, *Tectonophysics*, *339*,
618 495-510.

619 Ferrari, G. (1991), The 1887 Ligurian earthquake: a detailed study from contemporary scientific
620 observations, *Tectonophysics*, *193*, 131-139.

621 Fine, I. V., A. B. Rabinovitch, B. D. Bornhold, R. E. Thomson, and E. A. Kulikov (2005), The
622 Grand Banks landslide-generated tsunami of November 18, 1929: preliminary analysis
623 and numerical modeling, *Marine Geology*, *215*, 45-57.

624 Fryer, G. J., P. Watts, and L. F. Pratson (2004), Source of the great tsunami of 1 April 1946: a
625 landslide in the upper Aleutian forearc, *Marine Geology*, *203*, 201-218.

626 Garziglia, S., S. Migeon, E. Ducassou, L. Loncke, and J. Mascle (2008), Mass-transport
627 deposits on the Rosetta province (NW Nile Dea-sea turbidite system, Egyptian margin):
628 characteristics, distribution, and potential causal processes, *Marine Geology*, *250*, 180-
629 198.

630 Gennesseaux, M., A. Mauffret, and G. Pautot (1980), Les glissements sous-marins de la pente
631 continentale niçoise et la rupture de câbles en mer Ligure (Méditerranée occidentale),
632 *Comptes Rendus de l'Académie des Sciences Paris*, *290*, 959-962.

633 Goldfinger, C., L. D. Kulm, L. C. McNeill, and P. Watts (2000), Super-scale failure of the
634 southern Oregon Cascadia Margin, *Pure and Applied Geophysics*, *157*, 1189-1226.

635 Haflidason, H., H. P. Sejrup, A. Nygard, J. Mienert, P. Bryn, R. Lien, C. F. Forsberg, K. Berg,
636 and D. G. Masson (2004), The Storegga Slide: architecture, geometry and slide
637 development, *Marine Geology*, *213*, 201-234.

638 Hassoun, V., S. Migeon, A. Cattaneo, C. Larroque, and B. Mercier de Lepinay (2009),
639 Imbricated scars on the Ligurian continental slope: evidence for multiple failure events in
640 the 1887 earthquake epicentral area. International Conference on Seafloor Mapping for
641 Geohazard Assessment, 11-13 May 2009, Ischia (Italy). Rendiconti online della Società
642 Geologica Italiana, *7*, 113-117.

643 Hsu, K. J., M. B. Cita, and W. B. F. Ryan (1973), The origin of the Mediterranean evaporites, in
644 *Initial Reports DSDP*, edited, pp. 1203-1231, U.S. Govt. Printing Office, Washington
645 D.C.

646 Huhnerbach, V., and D. G. Masson (2004), Landslides in the North Atlantic and its adjacent
647 seas: an analysis of their morphology, setting and behaviour, *Marine Geology*, 213, 343-
648 362.

649 Imbo, Y., M. De Batist, M. Canals, M. J. Prieto, and J. Baraza (2003), The Gebra Slide: a
650 submarine slide on the Trinity Peninsula Margin, Antarctica, *Marine Geology*, 193, 235-
651 252.

652 Ioualalen, M., S. Migeon, and O. Sardou (2010), Landslide tsunami vulnerability in the
653 Ligurian Sea: case study of the October 16th 1979 Nice airport submarine landslide and
654 of identified geological mass failures, *Geophysical Journal International*, 181(2), 724-
655 740.

656 Jolivet, L., and C. Faccenna (2000), Mediterranean extension and the Africa-Eurasia collision,
657 *Tectonics*, 19(6), 1095-1106.

658 Klaucke, I., and P. Cochonat (1999), Analysis of past seafloor failures on the continental slope
659 off Nice (SE France), *Geo-Marine Letters*, 19, 245-253.

660 Klaucke, I., B. Savoye, and P. Cochonat (2000), Patterns and processes of sediment dispersal
661 on the continental slope off Nice, SE France, *Marine Geology*, 162, 405-422.

662 Kvalstad, T. J. (2007), What is the current "best practice" in offshore geohazard investigations?
663 A state-of-the-art review. Offshore Technology Conference, 30 April–3 May 2007,
664 Houston, TX, USA. OTC 18545, 14pp.

665 Laberg, J. S., T. O. Vorren, J. A. Dowdeswell, N. H. Kenyon, and J. Taylor (2000), The Andøya
666 Slide and the Andøya Canyon, north- eastern Norwegian–Greenland Sea, *Marine
667 Geology*, 162, 259-275.

668 Lamarche, G., C. Joanne, and J.-Y. Collot (2008), Successive, large mass-transport deposits in
669 the south Kermadec fore-arc basin, New Zealand: The Matakaoa Submarine Instability
670 Complex, *Geochemistry, Geophysics, Geosystems*, 9(4), 1-30.

671 Lambeck, K., and A. Purcell (2005), Sea-level change in the mediterranean Sea since the LGM:
672 model predictions for tectonically stable areas, *Quaternary Science Reviews*, 24, 1969-
673 1988.

674 Larroque, C., B. Mercier de Lepinay, and S. Migeon (this issue), Morphotectonic and faults-
675 earthquakes relationship along the northern Ligurian margin (Western Mediterranean)
676 based on high-resolution multibeam bathymetry and multichannel seismic reflection,
677 *Marine Geophysical Researches*.

678 Larroque, C., B. Delouis, B. Godel, and J.-M. Nocquet (2009), Active deformation at the
679 southwestern Alps - Ligurian basin junction (France-Italy boundary): Evidence for recent
680 change from compression to extension in the Argentera massif, *Tectonophysics*, 467, 1-4.

681 Larroque, C., N. Béthoux, C. Calais, F. Courboux, A. Deschamps, J. Déverchère, J.-F.
682 Stéphan, J.-F. Ritz, and E. Gilli (2001), Active and recent deformation at the Southern
683 Alps-Ligurian basin junction, *Netherland Journal of GeoSciences*, 80, 255-272.

684 Lastras, G., M. Canals, R. Urgeles, M. De Batist, A. M. Calafat, and J. L. Casamor (2004),
685 Characterisation of the recent BIG'95 debris flow deposit on the Ebro margin, Western
686 Mediterranean Sea, after a variety of seismic reflection data, *Marine Geology*, 213, 235-
687 255.

688 Lofi, J., C. Gorini, S. Berne, G. Clauzon, A. T. dos Reis, W. B. F. Ryan, and M. S. Steckler
689 (2005), Erosional processes and paleo-environmental changes in the western Gulf of
690 Lions (SW France) during the Messinian Salinity Crisis, *Marine Geology*, 217, 1-30.

691 López-Venegas, A. M., U. S. ten Brink, and E. L. Geist (2008), Submarine landslide as the
692 source for the October 11, 1918 Mona Passage tsunami: Observations and modeling,
693 *Marine Geology*, 254, 35-46.

694 Mascle, J., O. Sardou, L. Loncke, S. Migeon, L. Caméra, and V. Gaullier (2006),
695 Morphostructure of the Egyptian continental margin: Insights from swath bathymetry
696 surveys, *Marine Geophysical Researches*, 27, 49-59.

697 Maslin, M., M. Owen, S. Day, and D. Long (2004), Linking continental-slope failures and
698 climate change: testing the clathrate gun hypothesis, *Geology*, 32, 53-56.

699 Maslin, M., C. Vilela, N. Mikkelsen, and P. Grootes (2005), Causes of catastrophic sediment
700 failures of the Amazon Fan, *Quaternary Science Reviews*, 24, 2180-2193.

701 McAdoo, B. G., and P. Watts (2004), Tsunami hazard from submarine landslides on the Oregon
702 continental slope, *Marine Geology*, 203, 235-245.

703 McAdoo, B. G., L. F. Pratson, and D. L. Orange (2000), Submarine landslide geomorphology,
704 US continental slope, *Marine Geology*, 169, 103-136.

705 Migeon, S., T. Mulder, B. Savoye, and F. Sage (2006), The Var turbidite system (Ligurian Sea,
706 northwestern Mediterranean)-morphology, sediment supply, construction of turbidite
707 levee and sediment waves: implication for hydrocarbon reservoirs, *Geo-Marine Letters*,
708 26, 361-371.

709 Migeon, S., B. Savoye, E. Zanella, T. Mulder, J.-C. Faugères, and O. Weber (2001), Detailed
710 seismic-reflection and sedimentary study of turbidite sediment waves on the Var
711 Sedimentary Ridge (SE France): significance for sediment transport and deposition and
712 for the mechanisms of sediment-wave construction, *Marine and Petroleum Geology*, 18,
713 179-208.

714 Moore, J. G., D. A. Clague, R. T. Holcomb, P. W. Lipman, W. R. Normark, and M. E. Torresan
715 (1989), Prodigious submarine landslides on the Hawaiian Ridge, *Journal of Geophysical*
716 *Research*, 94(B12), 17,465-417,484.

717 Mulder, T., B. Savoye, and J. P. M. Syvitski (1997), Numerical modelling of a mid-sized
718 gravity flow: the 1979 Nice turbidity current (dynamics, processes, sediment budget and
719 seafloor impact), *Sedimentology*, 44, 305-326.

720 Mulder, T., B. Savoye, J. P. M. Syvitski, and O. Parize (1996), Des courants de turbidité
721 hyperpycniaux dans la tête du canyon du Var ? Données hydrologiques et observations de
722 terrain, *Oceanologica Acta*, 20, 607-626.

723 Mulder, T., B. Savoye, D. J. W. Piper, and J. P. M. Syvitski (1998), The Var submarine
724 sedimentary system: understanding Holocene sediment delivery processes and their
725 importance to the geological record, in *Geological processes on Continental Margins:
726 Sedimentation, Mass-Wasting and Stability*, edited by M. S. Stocker, D. Evans and A.
727 Cramp, pp. 146-166, Geological Society Special Publication, London.

728 Mulder, T., S. Migeon, B. Savoye, and J.-C. Faugeres (2001a), Inversely graded turbidite
729 sequences in the deep Mediterranean: a record of deposits from flood-generated turbidity
730 currents?, *Geo-Marine letters*, 21, 86-93.

731 Mulder, T., S. Migeon, B. Savoye, and J.-M. Jouanneau (2001b), Twentieth century floods
732 recorded in the deep Mediterranean sediments, *Geology*, 29(11), 1011-1014.

733 Piper, D. J. W., and B. Savoye (1993), Processes of late Quaternary turbidity current flow and
734 deposition on the Var deep-sea fan, north-west Mediterranean Sea, *Sedimentology*, 40,
735 557-582.

736 Piper, D. J. W., P. Cochonat, and M. L. Morrison (1999), The sequence of events around the
737 epicentre of the 1929 Grand Banks earthquake: initiation of debris flows and turbidity
738 current inferred from sidescan sonar, *Sedimentology*, 46, 79-97.

739 Piper, D. J. W., D. C. Mosher, B.-J. Gauley, K. A. Jenner, and D. C. Campbell (2003), The
740 chronology and recurrence of submarine mass movements on the continental slope off
741 southeastern Canada, in *Submarine mass movements and their consequences*, edited by J.
742 Locat and J. Mienert, pp. 299-306, Kluwer Academic Publishers,
743 Dordrecht/Boston/London.

744 Piper, D. J. W., C. Pirmez, P. L. Manley, D. Long, R. D. Flood, W. R. Normark, and W.
745 Showers (1997), Mass-transport deposits of the Amazon Fan, in *Proceedings of the*
746 *Ocean Drilling Program, Scientific Results*, edited by R. D. Flood, D. J. W. Piper, A.
747 Klaus and L. C. Peterson, pp. 109-146.

748 Réhault, J.-P., G. Boillot, and A. Mauffret (1984), The western Mediterranean basin geological
749 evolution, *Marine Geology*, 55, 447-477.

750 Rollet, N., J. Déverchère, M.-O. Beslier, P. Guennoc, J.-P. Réhault, M. Sosson, and C. Truffert
751 (2002), Back arc extension, tectonic inheritance and volcanism in the Ligurian sea,
752 Western Mediterranean, *Tectonics*, 21.

753 Sage, F., G. Von Gronefeld, J. Déverchère, V. Gaullier, A. Maillard, and C. Gorini (2005),
754 Seismic evidence for Messinian detrital deposits at the western Sardinia margin,
755 northwestern Mediterranean, *Marine and Petroleum Geology*, 22, 757-773.

756 Savoye, B., and D. J. W. Piper (1991), The Messinian event on the margin of the Mediterranean
757 Sea in the Nice area, southern France, *Marine Geology*, 97, 279-304.

758 Savoye, B., D. J. W. Piper, and L. Droz (1993), Plio-Pleistocene evolution of the Var deep-sea
759 fan off the French Riviera, *Marine and Petroleum Geology*, 10, 550-571.

760 St-Onge, G., T. Mulder, D. J. W. Piper, C. Hillaire-Marcel, and J. S. Stoner (2004), Earthquake
761 and flood-induced turbidites in the Saguenay Fjord (Québec): a Holocene paleoseismicity
762 record, *Quaternary Science Reviews*, 23, 283-294.

763 Strzeczynski, P., J. Déverchère, A. Cattaneo, A. Domzig, K. Yelles, B. Mercier de Lepinay, N.
764 Babonneau, and A. Boudiaf (2010), Tectonic inheritance and Pliocene-Pleistocene
765 inversion of the Algerian margin around Algiers: Insights from multibeam and seismic
766 reflection data, *Tectonics*, 29. TC2008, doi: 10.1029/2009TC002547

767 Sultan, N., P. Cochonat, J.-P. Foucher, and J. Mienert (2004a), Effect of gas hydrates melting on
768 seafloor slope instability, *Marine Geology*, 213, 379-401.

769 Sultan, N., et al. (2004b), Triggering mechanisms of slope instability processes and sediment
770 failures on continental margins: a geotechnical approach, *Marine Geology*, 213, 291-321.

771 ten Brink, U. S., H. J. Lee, E. L. Geist, and D. C. Twichell (2009), Assessment of tsunami
772 hazard to the U.S. East Coast using relationships between submarine landslides and
773 earthquakes, *Marine Geology*, 264, 65-73.

774 Urgeles, R., M. Canals, J. Baraza, B. Alonso, and D. G. Masson (1997), The most recent
775 megalandslides of the Canary Islands: El Golfo debris avalanche and Canary debris flow,
776 west El Hierro Island, *Journal of Geophysical Research*, 102(B9), 20,305-320,323.

777
778
779

780 Figure caption

781 Figure 1: General shaded bathymetric map of the northern Ligurian margin collected during the
782 MALISAR project between the cities of Nice (France) to Genova (Italy). (A) and (B) are
783 bathymetric profiles. FS are fault scarps observed south of the Imperia Promontory. Location of
784 Figures 2 and 12 is also shown.

785 Figure 2: Shaded bathymetric map illustrating the morphology of the western Ligurian margin
786 and the location and distribution of the three types of failures identified. The dark dashed lines
787 at the base of the continental slope illustrate the location of faults identified on the seismic-
788 reflection profiles. Map location shown in Figure 1.

789 Figure 3: A) Shaded bathymetric map illustrating the morphology of failures of Type 1 located
790 on the upper part of the continental slope offshore the Var and Paillon rivers. B) Shaded
791 bathymetric map illustrating the morphology of failures of Type 1 in and nearby the epicentral
792 area of the 1887 earthquake. The inset shows a scar and a MTD. The white dotted lines
793 underline the contour of the scars. Location in Figure 2.

794 Figure 4: Shaded bathymetric map illustrating the morphology of failures of Type 2 located at
795 the base of the continental slope in the western part of the Ligurian margin. The white dotted
796 lines reveal the contour of the accumulation of debris identified at the foot of the failures. (1) is
797 a bathymetric profile crossing longitudinally the Cirque Marcel. The white dashed line is the
798 location of the bathymetric profile. Location of Figures 5 and 6A is also shown.

799 Figure 5: Side-scan sonar data collected in a failure of Type 2. Profile location shown in Figure
800 4. A) Seafloor image revealing the presence of small-scale scours affecting some of the scars
801 within the failure area and of bloks (B) several tens of meters in diameter at the foot of the
802 failure. B) 3.5 kHz profile illustrating the step-like morphology of the scars and the presence of
803 an accumulation of debris at the foot of the failure.

804 Figure 6: A) Side scan sonar image collected at the base of the continental slope and revealing
805 the presence of a fault escarpment on the seafloor. Image location shown in Figure 4. B) Side
806 scan sonar image showing a fault escarpment at the base of the continental slope and the
807 presence of bloks (B) several tens of meters in diameter located at the foot of some scar
808 failures. Image location shown in Figure 2.

809 Figure 7: Seismic-reflection profile crossing a Type-2 failure at the base of the continental slope
810 in the western Ligurian margin. Note the faults affecting the base of the continental slope. Profile
811 location shown in Figure 2.

812 Figure 8: General shaded bathymetric map of the western part of the VSR. The white continuous
813 line follows the contour of the main scar. The white dotted line outlines the presence of small-
814 scale scars separated by elongated ridges on the inner wall of the main scar. Location of Figures
815 9, 10 and 11 is also shown.

816 Figure 9: Strike seismic-reflection profile collected across the failure area identified in the
817 western part of the VSR. It locates on top of faults with a flower-like structure. Undisturbed
818 deposits of the VSR are characterized by a well-layered acoustic facies. Two paleochannels and
819 the top of the Messinian evaporites are identified at depth and are affected by faults taking root in
820 the evaporites. Profile location shown in Figure 8.

821 Figure 10: Dip seismic-reflection profile collected across the crest of the VSR and the failure
822 area. Surficial deposits of the VSR are affected that syn-sedimentary faults that prolonged at
823 depth by larger normal faults affecting some paleochannels and the Messinian evaporites. Profile
824 location shown in Figure 8.

825 Figure 11: Hull-mounted Chirp profiles collected in the western part of the VSR and showing
826 the presence of a lenticular transparent unit in the continuity of the Type-3 failure identified in
827 Figures 8, 9 and 10. The transparent unit is interpreted as an MTD. Profile location shown in
828 Figure 8.

829 Figure 12: Shaded bathymetric map illustrating the morphology of the upper continental slope
830 in the Gulf of Genova. The white dotted line follows the edge of the Portofino Slide. Figure
831 location shown in Figure 2.

832 Figure 13: Shaded bathymetric map showing the morphology of the Finale Slide, located in the
833 interfluvium between the Pora and Noli canyons. The white dotted line follows the top of the main
834 scar. The white lines are the location of Chirp profiles from Figure 14. Figure location shown in
835 Figure 12.

836 Figure 14: Chirp profiles showing the presence of a chaotic to transparent unit downstream
837 from the scar of the Finale Slide. The unit is interpreted as a MTD related to the failure. Profile
838 location shown in Figure 13.

839

Fig. 1

[Click here to download high resolution image](#)

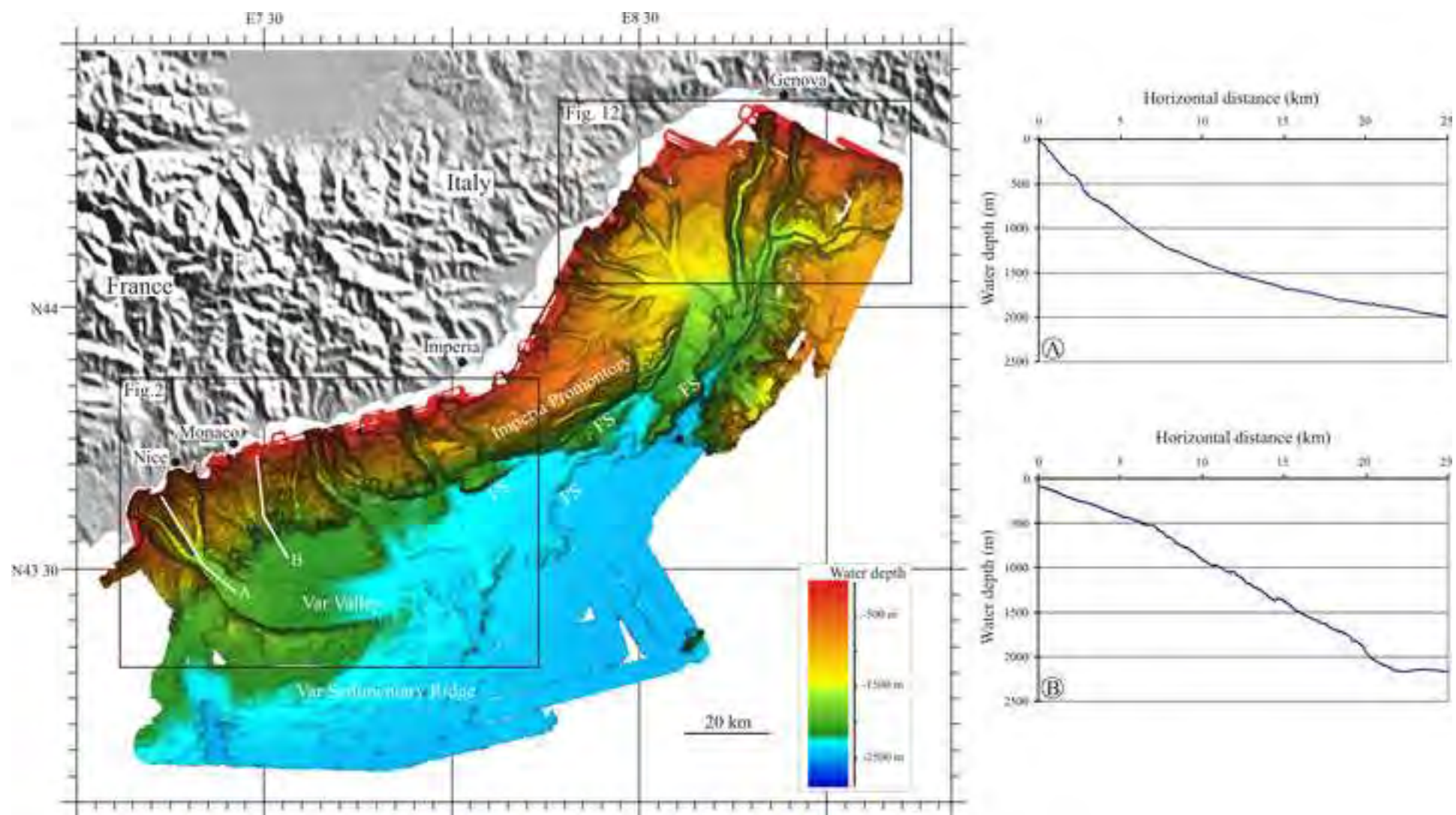


Fig. 2

[Click here to download high resolution image](#)

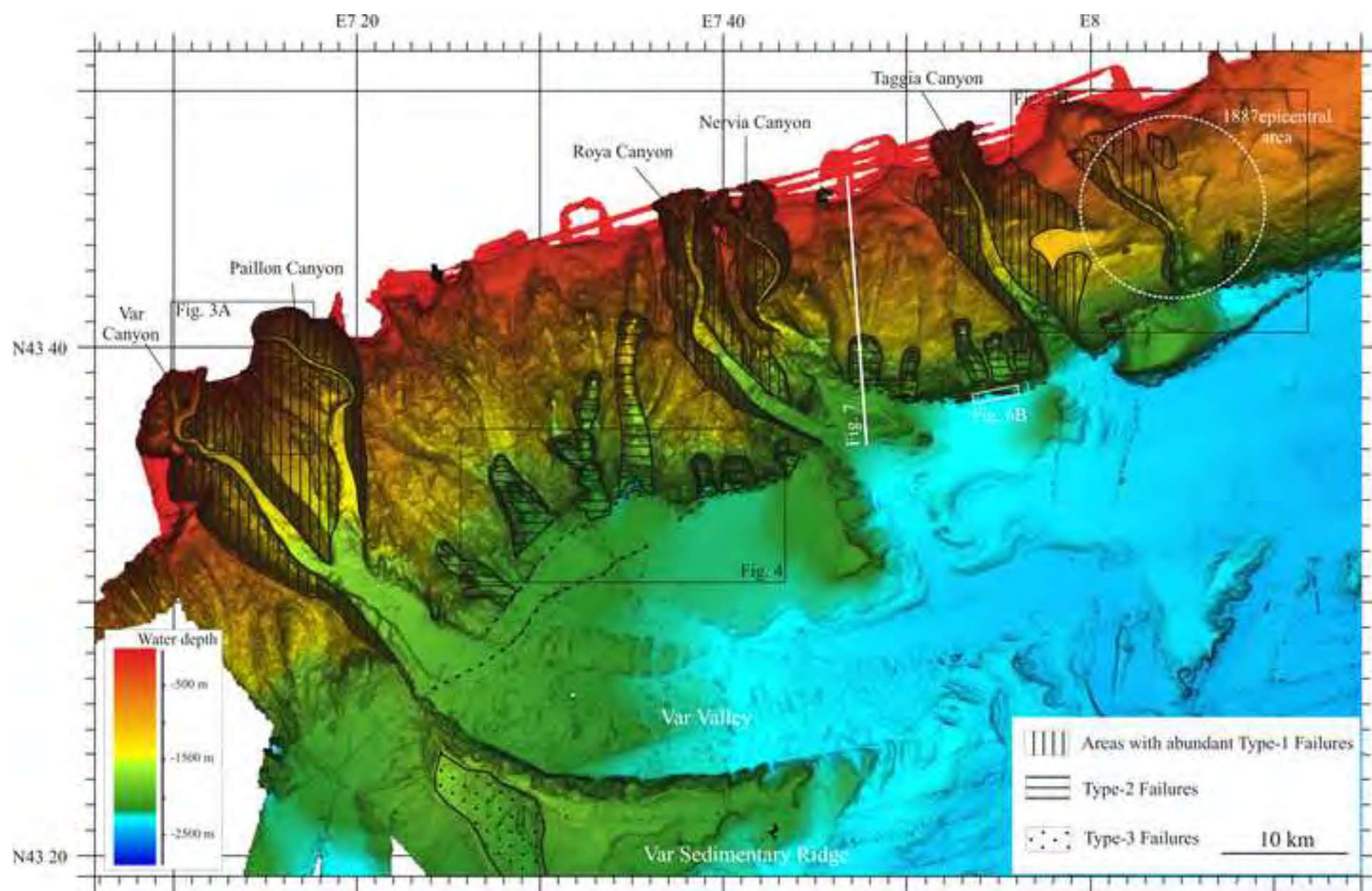


Fig. 3

[Click here to download high resolution image](#)

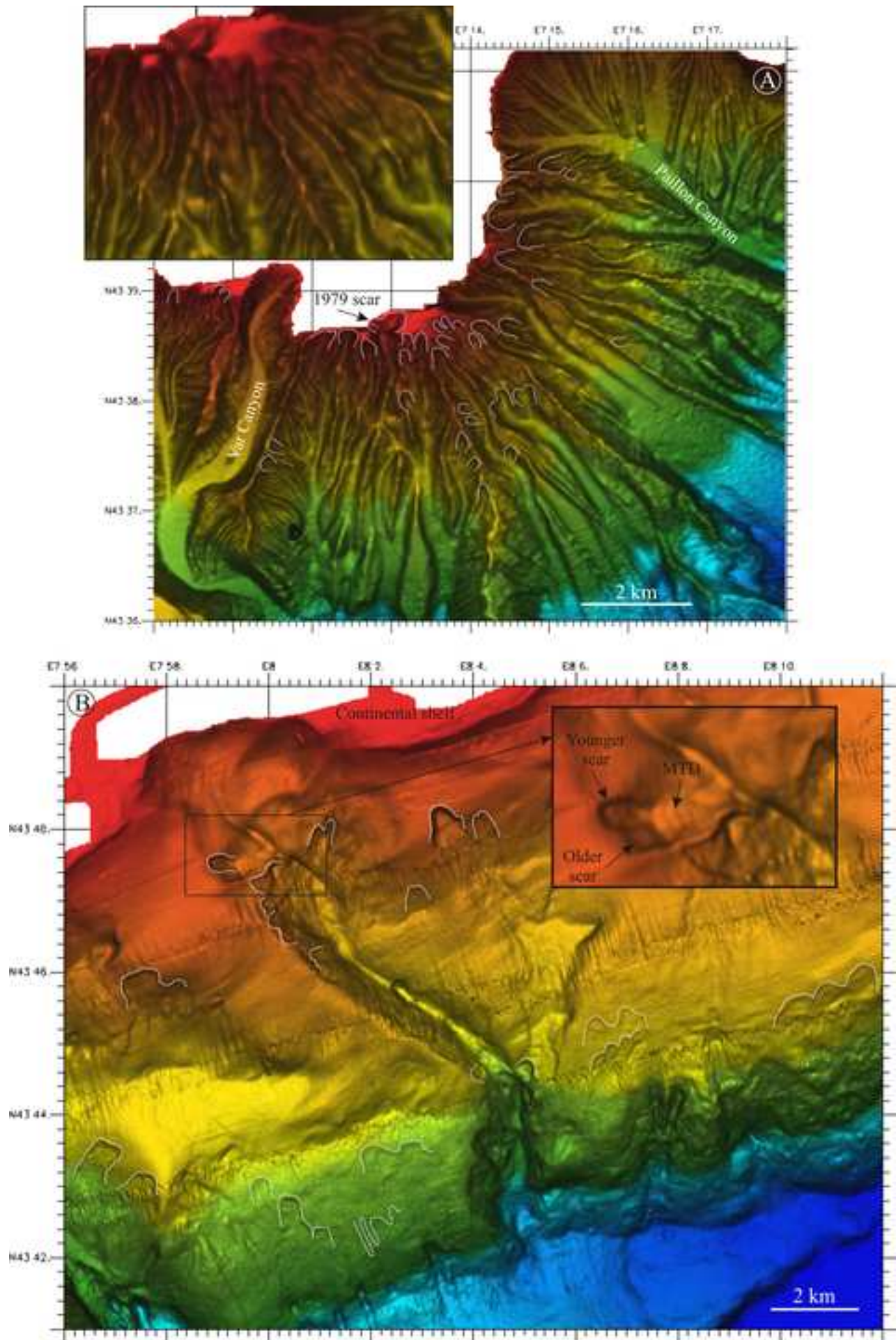
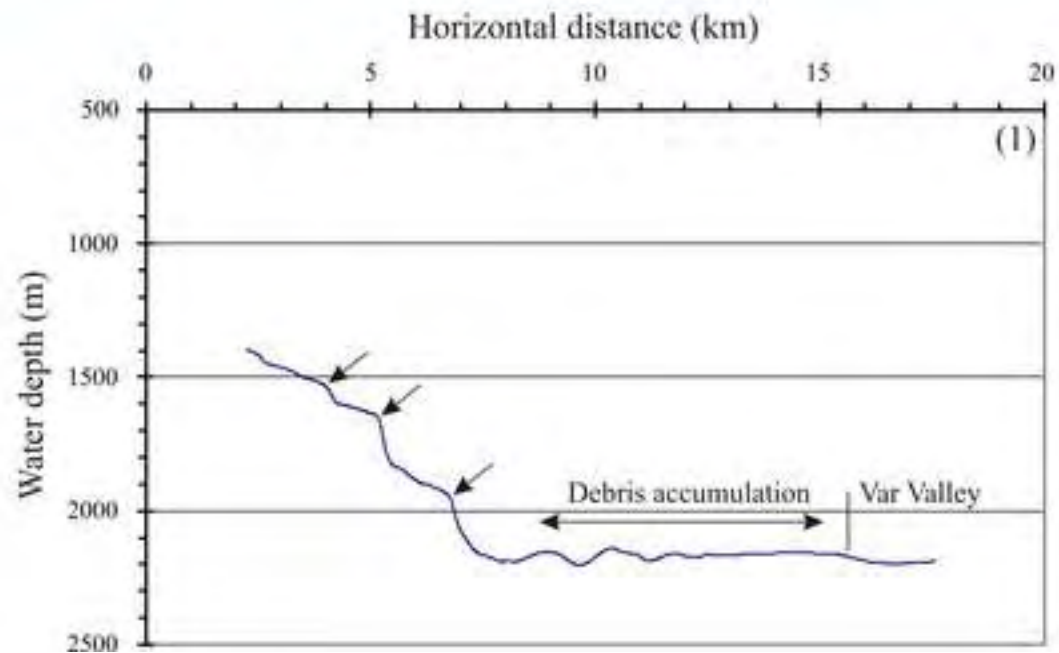
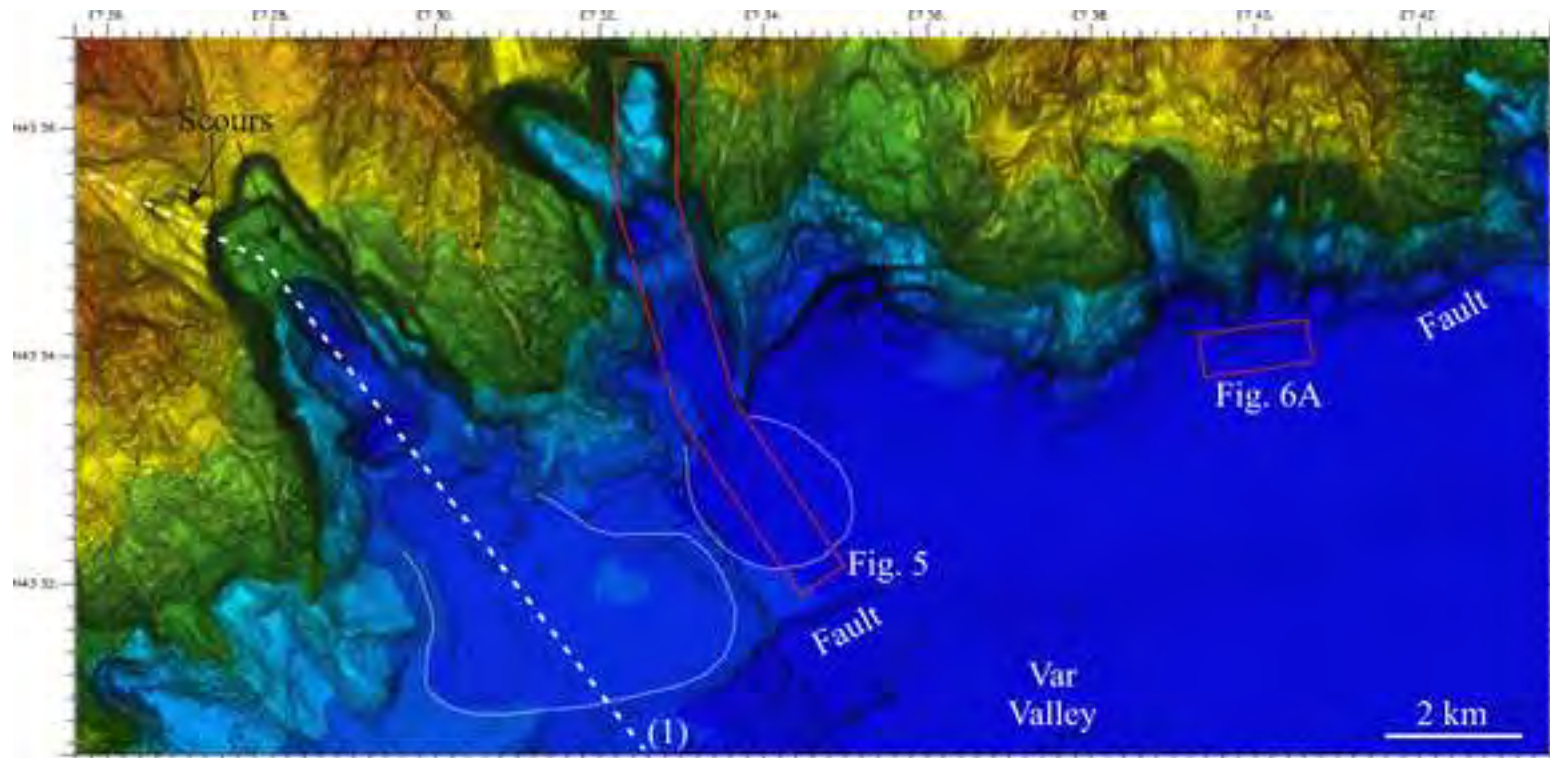
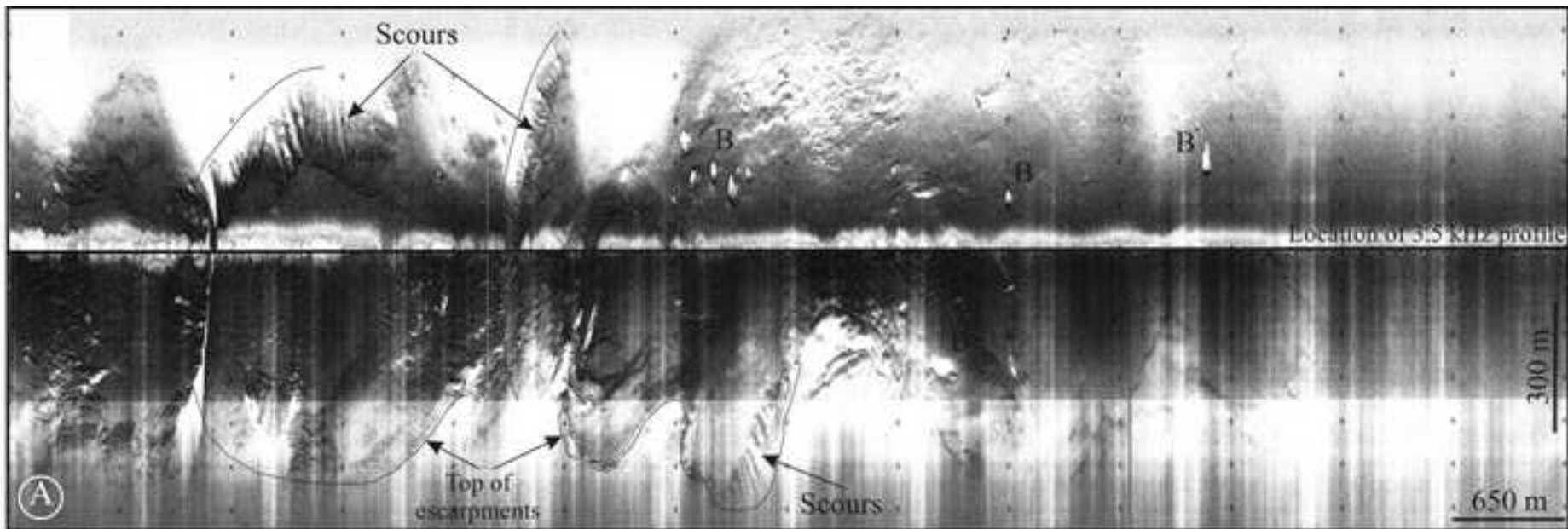


Fig. 4

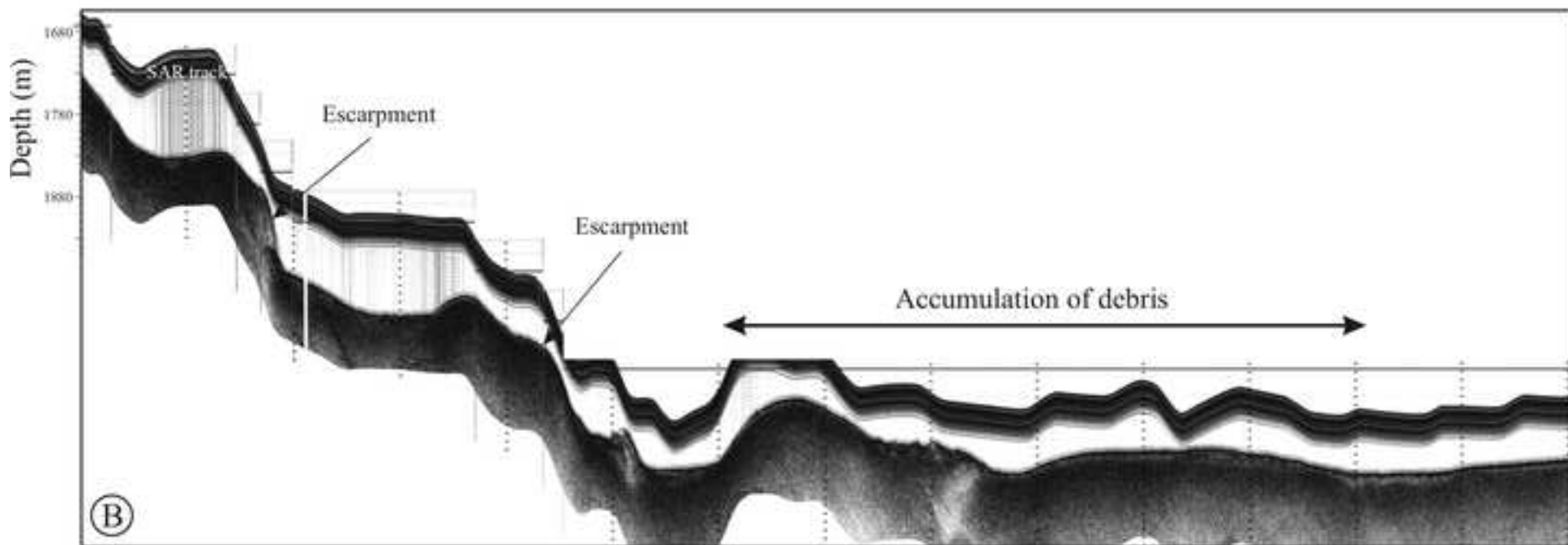
[Click here to download high resolution image](#)





North

South



(B)

Fig. 5 [Click here to download high resolution image](#)

Fig. 6

[Click here to download high resolution image](#)

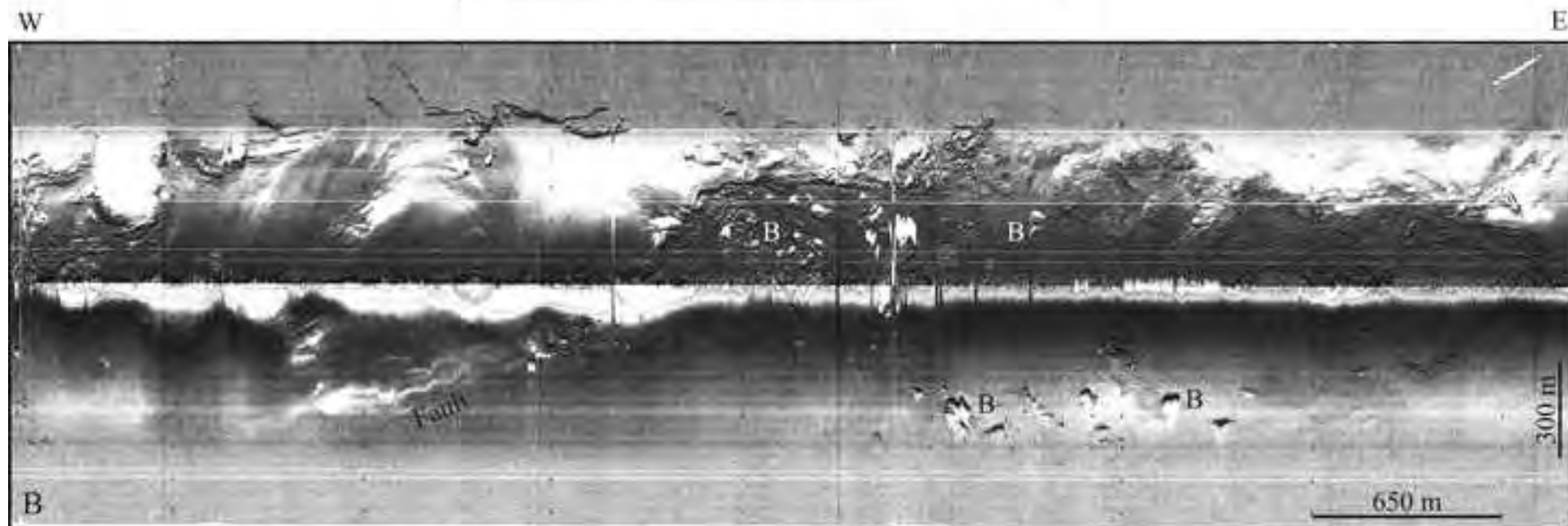
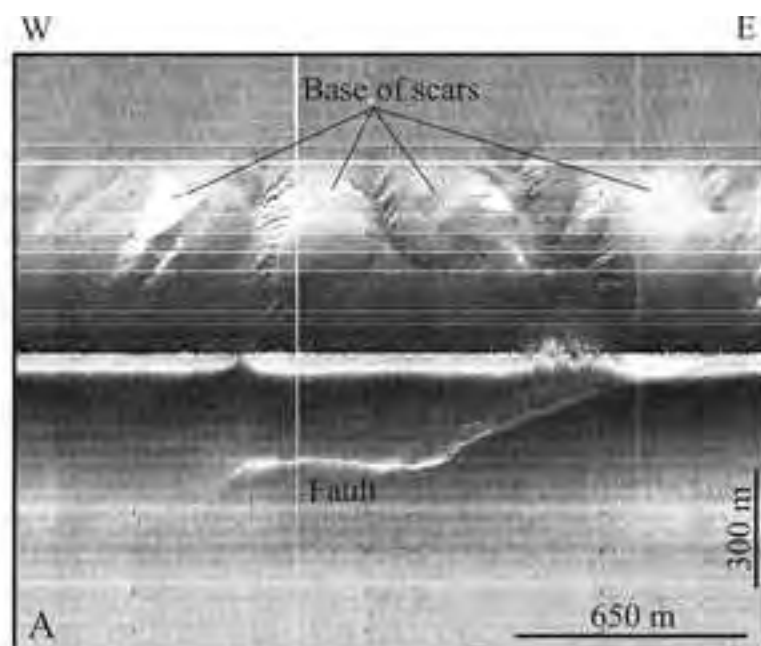


Fig. 7

[Click here to download high resolution image](#)

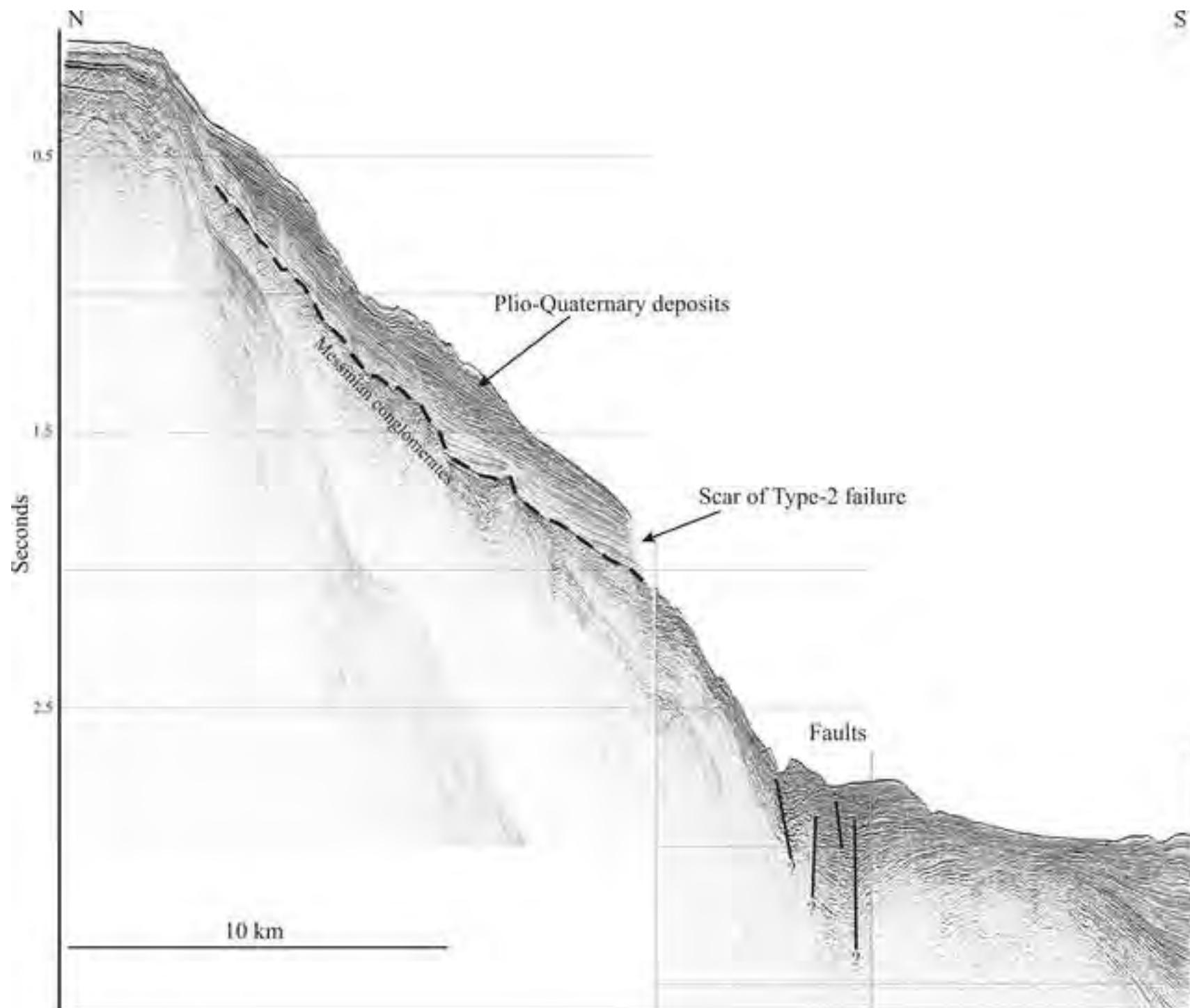


Fig. 8

[Click here to download high resolution image](#)

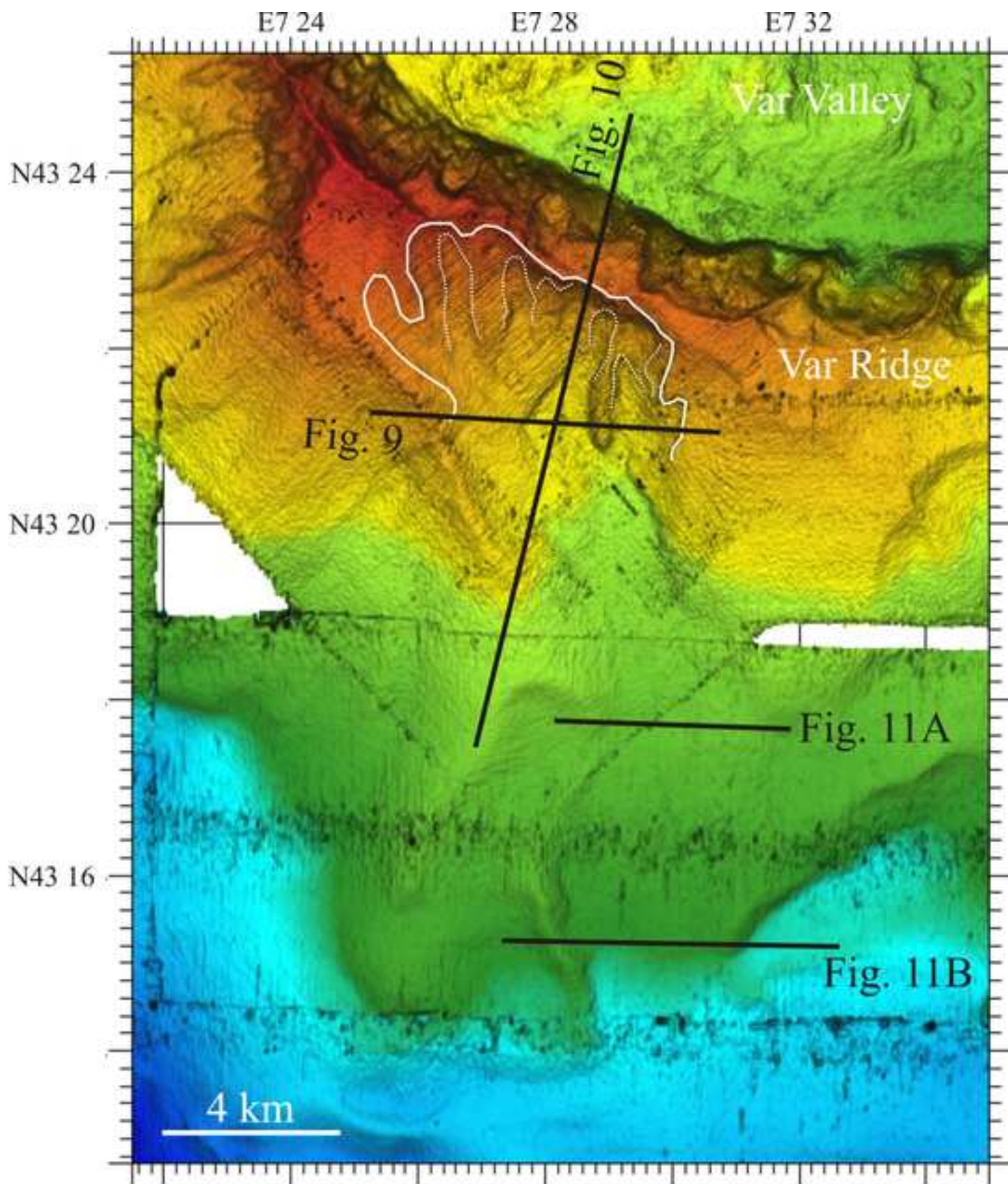


Fig. 9

[Click here to download high resolution image](#)

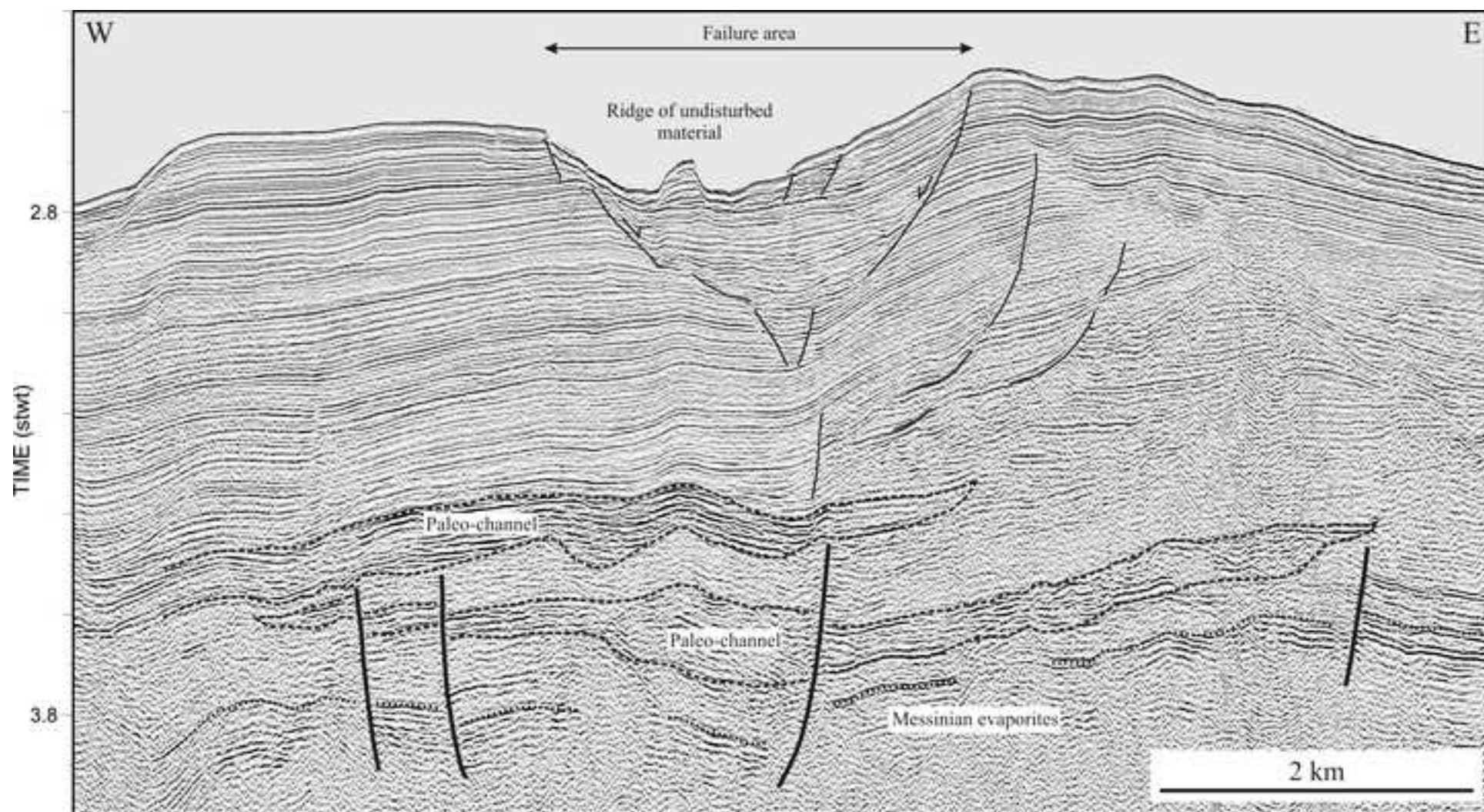


Fig. 10
[Click here to download high resolution image](#)

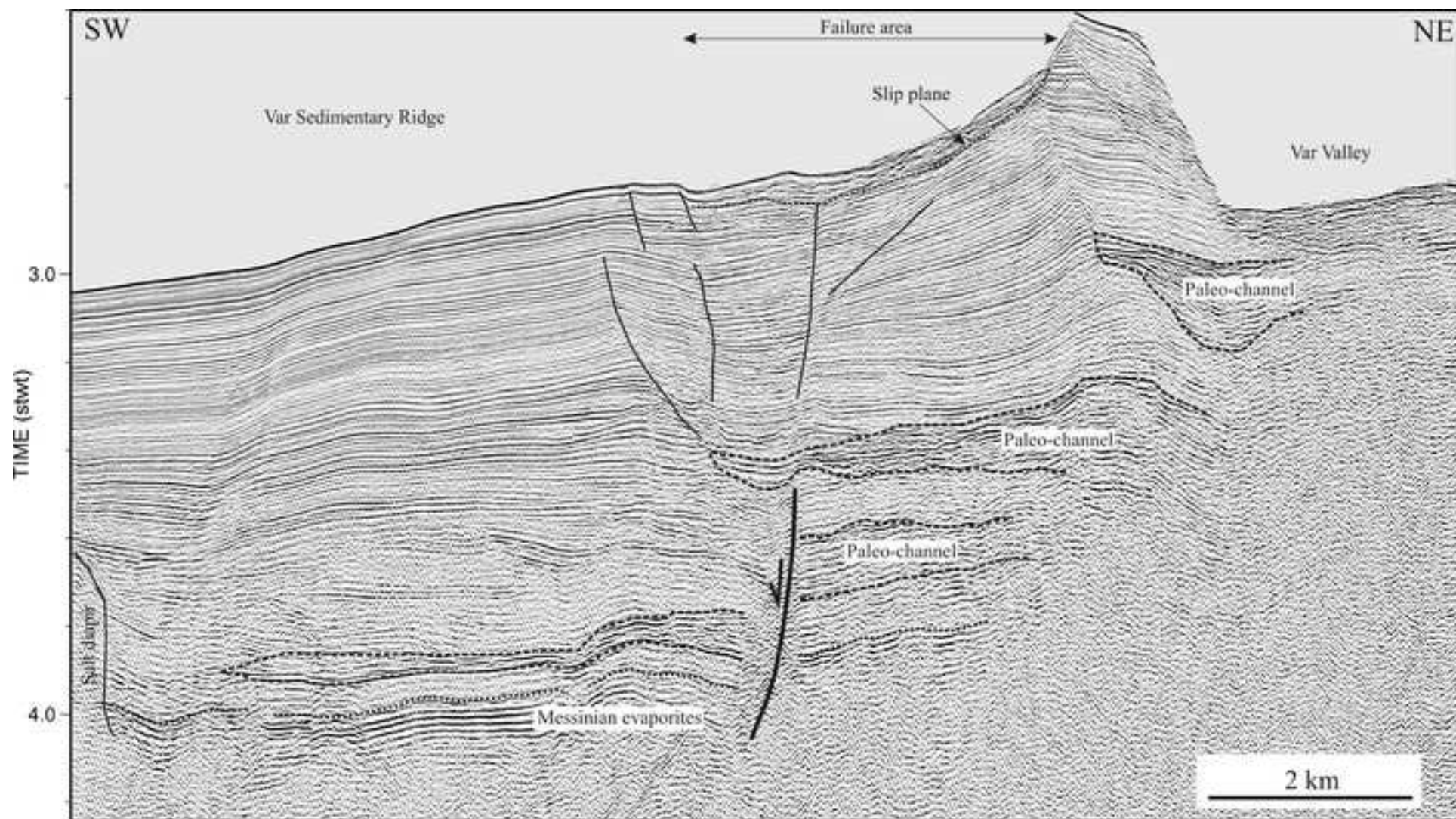


Fig. 11
[Click here to download high resolution image](#)

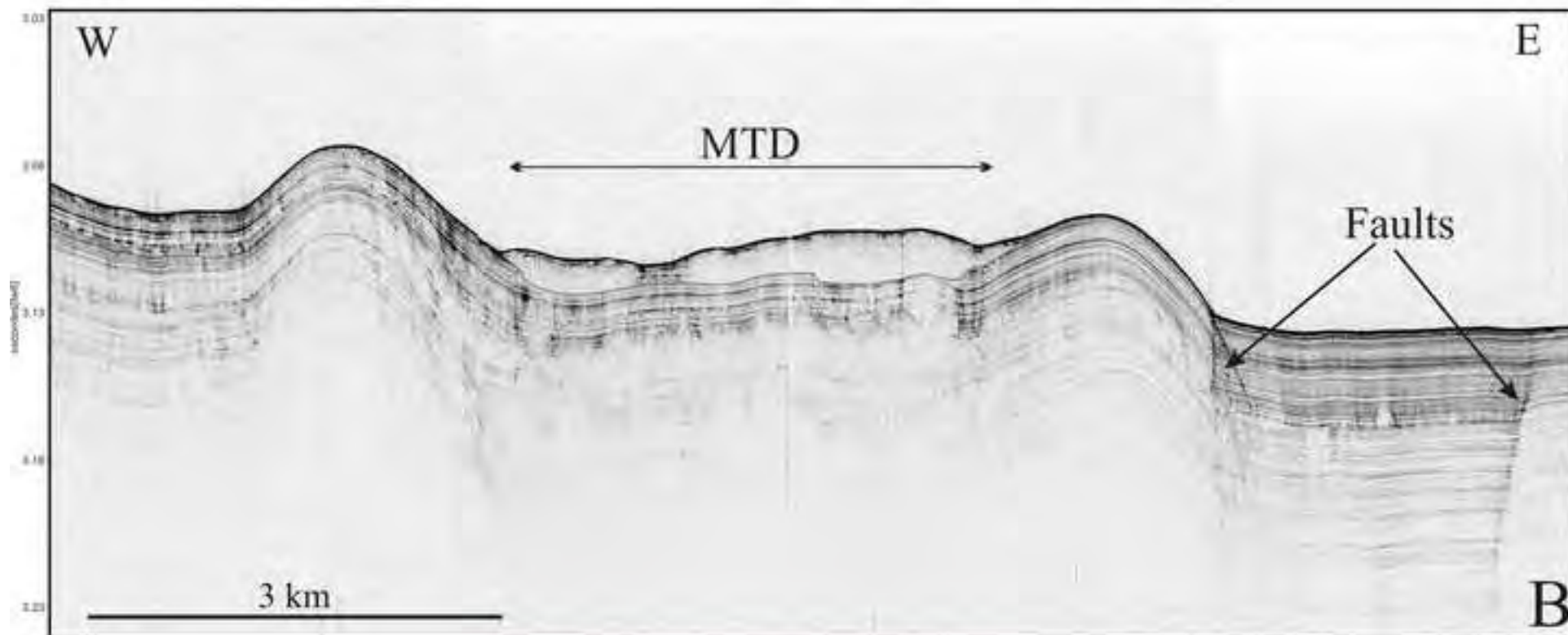
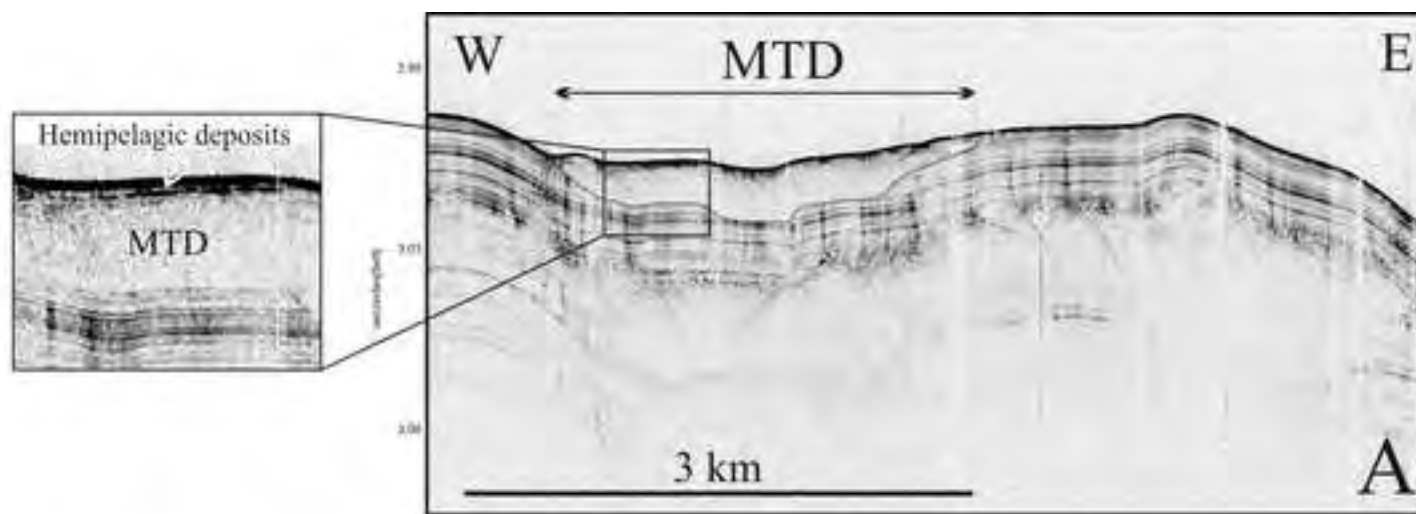


Fig. 12
[Click here to download high resolution image](#)

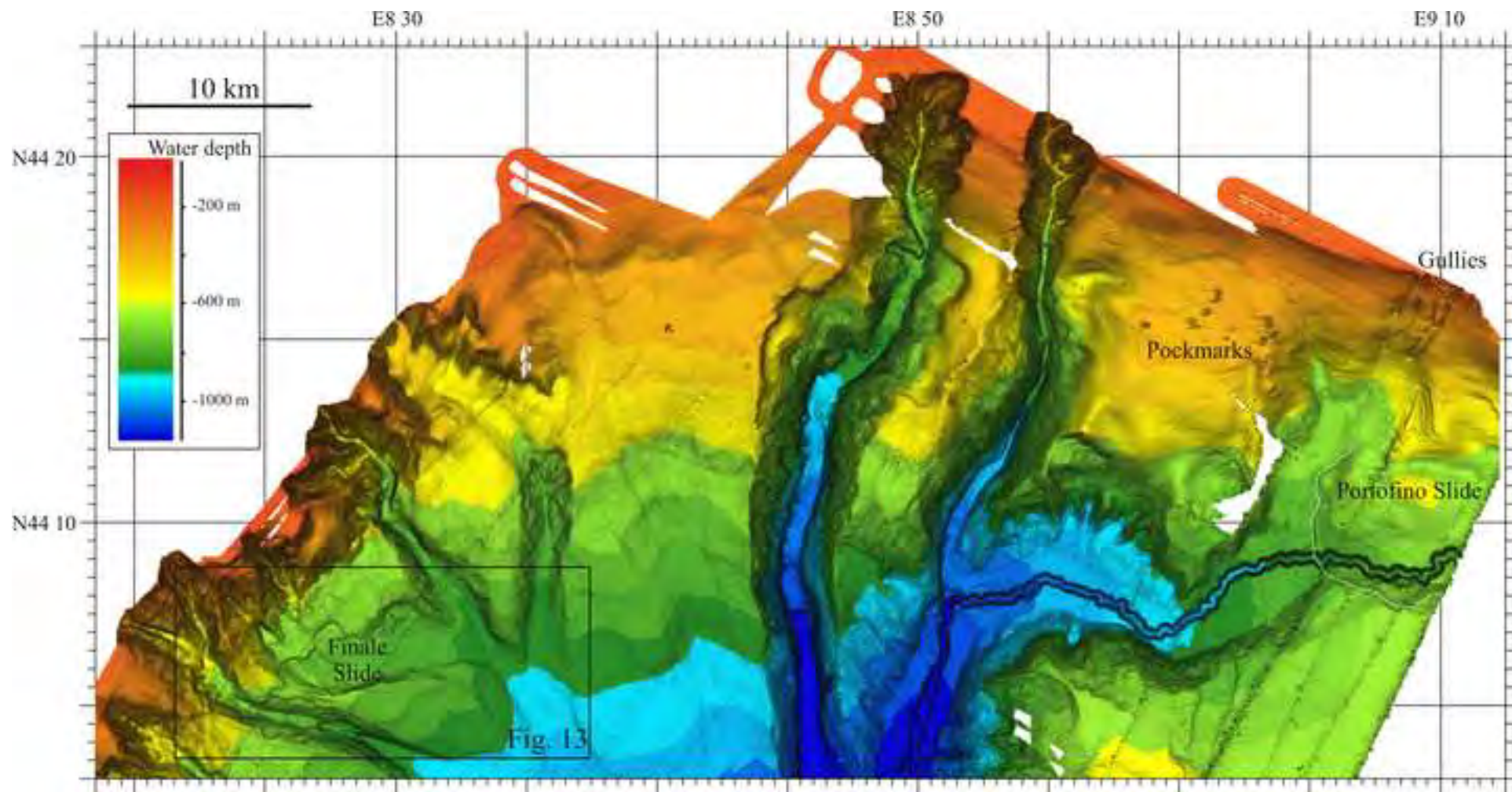


Fig. 13
[Click here to download high resolution image](#)

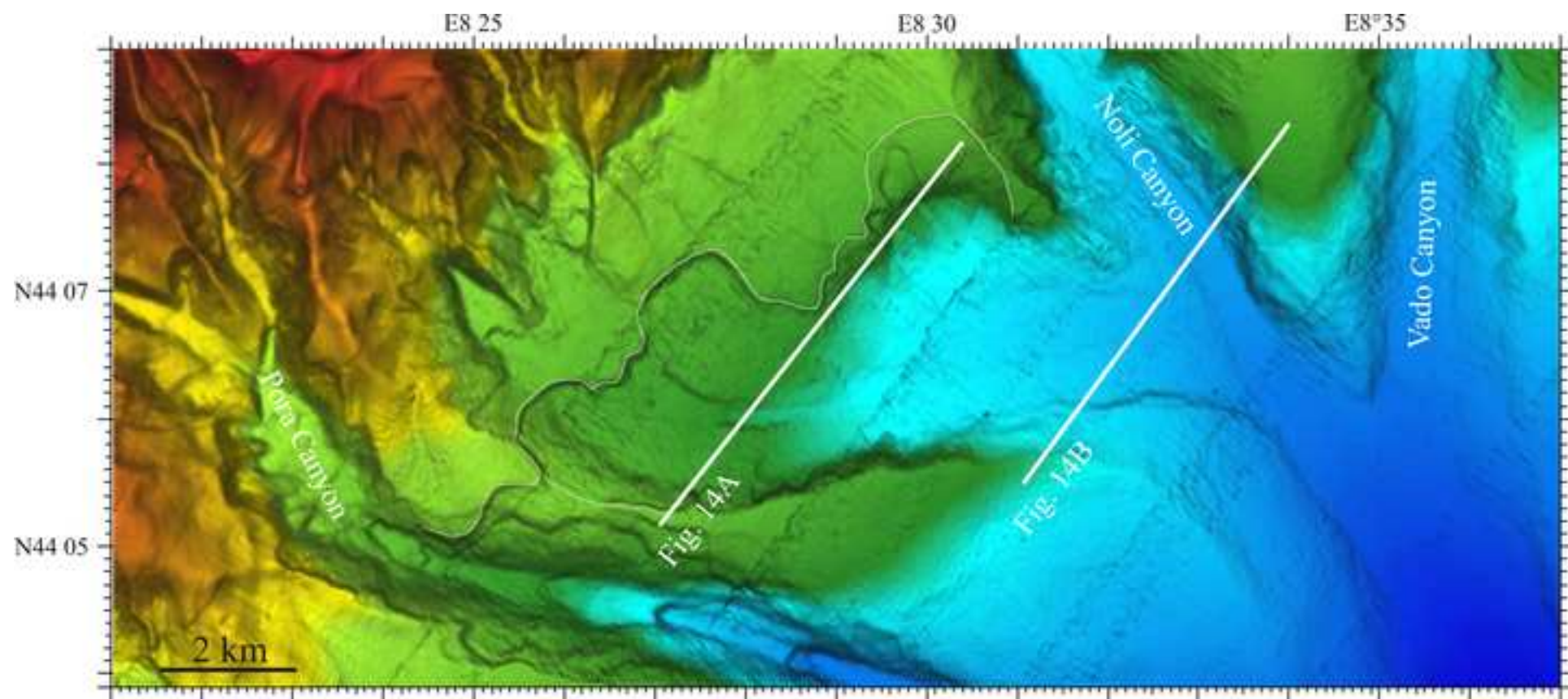


Fig. 14
[Click here to download high resolution image](#)

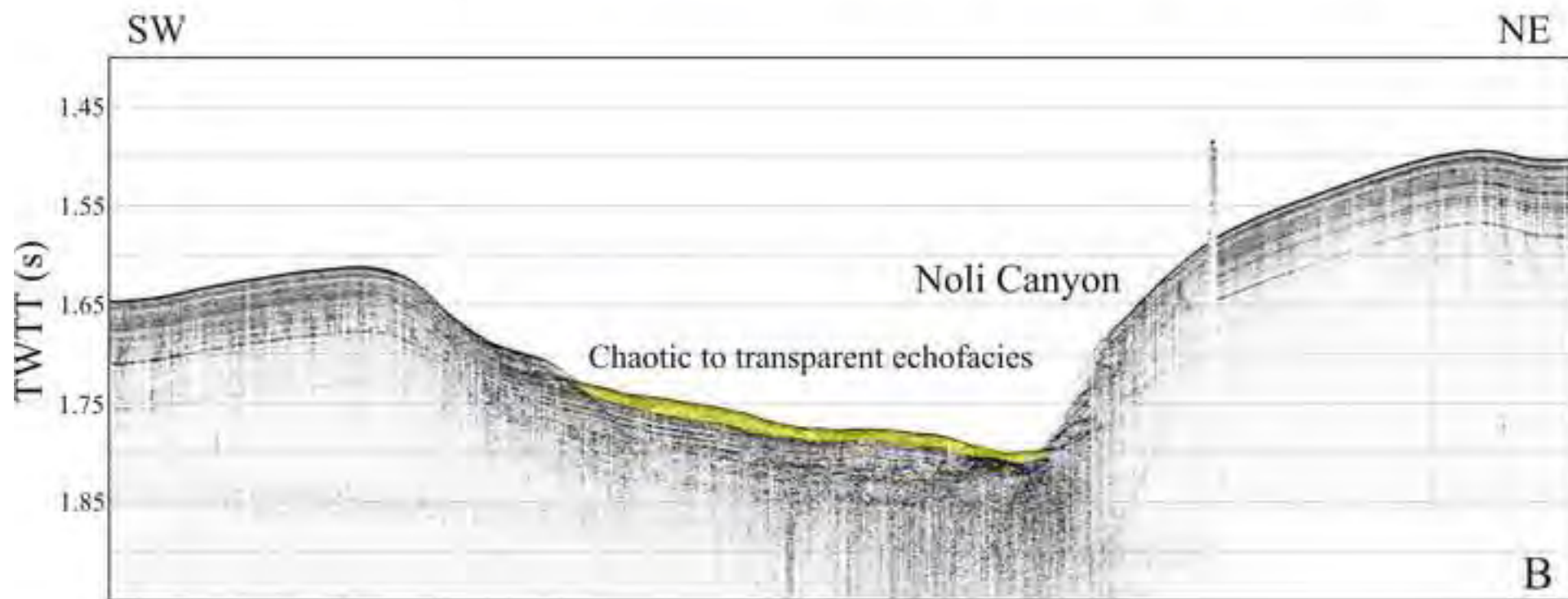
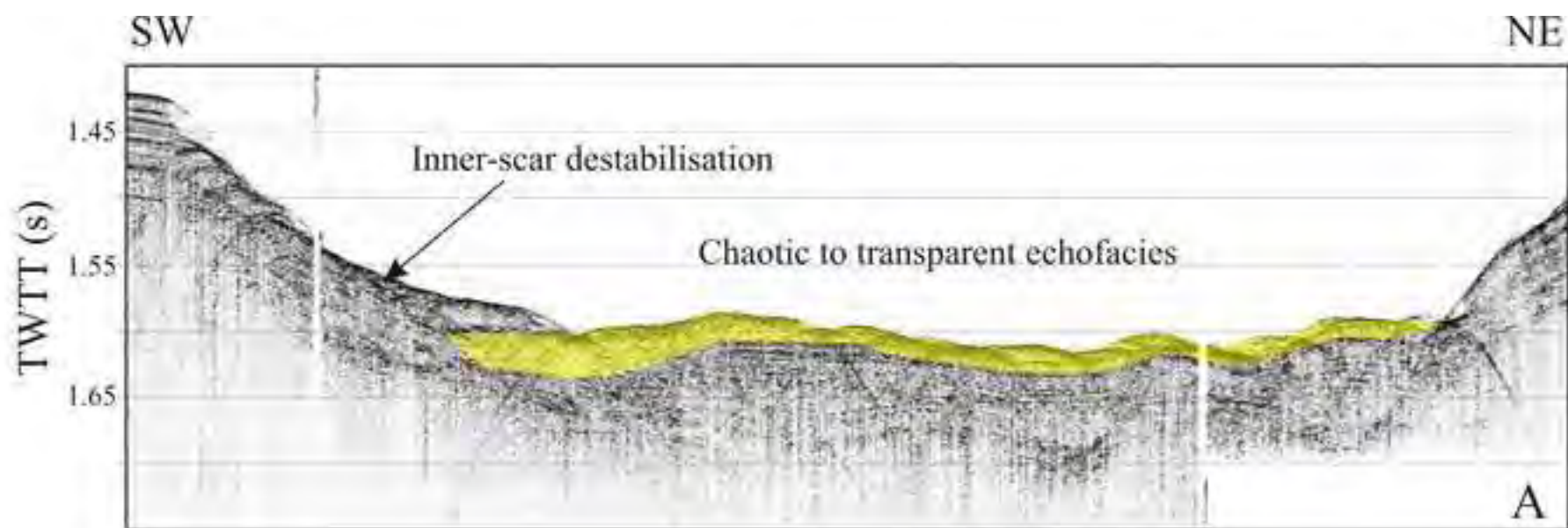


table 1[Click here to download table: Table1.doc](#)

	Type-1 scars	Type-2 scars	Type-3 scars
Number of studied scars	> 400	14	3
Examples	1979 Nice-airport landslide	‘Cirque Marcel’	VSR Slide Finale Slide Portofino Slide
Water-depth range (m)	0-2000	1700-2200	250-2100
Preferential location	Shelf edge, upper continental slope, canyon walls	Base of continental slope	Continental slope, deep basin
Size (H-W-L)	Small	Medium/large	Medium/large
Length	Few hundreds of meters	4-6 km	3-5 km
Width	100-400 m	2-4 km	6-10 km
Height	30-90 m	100-500 m	50-300 m
Volume	< 0,1 km ³	1 to 3 km ³	1 to 3 km ³
Regional slope	10-20°	6°	< 4°
Associated with	River mouths, erosional chutes	Faults, accumulations of debris	MTD
Main process	Mass wasting, disintegration process	Mass wasting, disintegration process	mass wasting
Potential geohazard associated	Low to high : tsunami, cable brakes	High : tsunami	Low : submarine landslide High : tsunami

Table 1: Summary of the main characteristics of each type of failure scars identified on the Ligurian margin.